[Supporting Information]

Novel Ionophores with 2n-Crown-n Topology: Anion Sensing via Pure Aliphatic C-H···A$^-$ Hydrogen Bonding

Genggongwo Shi,[1] Changdev Gadhe,[2] Sung-Woo Park,[1] Kwang S. Kim,[1] Jongmin Kang,[3] Humaira Seema,[1] N. Jiten Singh,[1] and Seung Joo Cho[2,3,*]

[1]Department of Chemistry, Pohang University of Science and Technology, Pohang, 790-784, Korea,
[2]Department of Bio-new-drug Development, Chosun University, Korea, chosj@chosun.ac.kr,
[3]Department of Chemistry, Sejong University, Seoul 143-747, South Korea
[4]Department of Cellular·Molecular Medicine, College of Medicine, Chosun University, 375 Seosuk-dong, Dong-gu, Gwangju 501-759, Korea
chosj@chosun.ac.kr

CONTENTS

1. General Experimental

General experimental methods. All common reagents and solvents were purchased and used without further purification. All reagents and NMR solvents were purchased from Sigma-Aldrich. The NMR solvent d6-benzene for titration is anhydrous level. All products were characterized by ^{1}H and ^{13}C NMR, performed on a Bruker Advance DPX500 (500 MHz) spectrometer at 298 K.

(2s,4s,6s)-2,4,6-tris(chloromethyl)-1,3,5-trioxane (3). Chloroacetaldehyde solution (~50 wt. % in H_2O) (12 g, 0.076 mol) was extracted by diethyl ether and the organic layers were combined. After evaporating diethyl ether under reduced pressure, the remained liquid was diluted by 20 mL of n-hexane and cooled to 0 °C. Maintaining the same temperature, concentrated sulfuric acid (3 mL) was added slowly with vigorous stirring continuing for 3 hours. Then the solid was collected by filtration, washed with water, and recrystallized from n-hexane to afford colorless needles of **3** (2.4 g, 0.010 mol, 40% yield). ^{1}H NMR (500 MHz, C_6D_6): δ 3.10 - 3.11 (d, 6H), 4.32 - 4.34 (t, 3H). ^{13}C NMR (500MHz, C_6D_6): δ 43.48, 99.88.

(2s,4s,6s)-2,4,6-tris(dichloromethyl)-1,3,5-trioxane (4). Dichloroacetaldehyde hydrate (3.0 g, 0.023mol) was slowly added to the cooled (0 °C) concentrated sulfuric acid (30 g) and vigorously stirred for 3 hours at 0 °C. The white solid was collected by sand core funnel, washed with water and recrystallized from methanol to afford white crystal of **4** (0.6 g, 1.8 mmol, 23% yield). ^{1}H NMR (500 MHz, C_6D_6): δ 4.29 – 4.30 (d, 3H), 5.02 – 5.03 (d, 3H). ^{13}C NMR (500MHz, C_6D_6): δ 69.01, 100.12.

(2s,4s,6s)-2,4,6-tris(trichloromethyl)-1,3,5-trioxane (5). The same procedure of synthesis of **3** was applied, using chloral hydrate as starting material. White solid of **5** was obtained (29% yield). ^{1}H NMR (500 MHz, C_6D_6): δ 8.08 (s, 3H). ^{13}C NMR (500MHz, C_6D_6): δ 94.70, 95.98.

2. ^{1}H, ^{13}C NMR Spectra

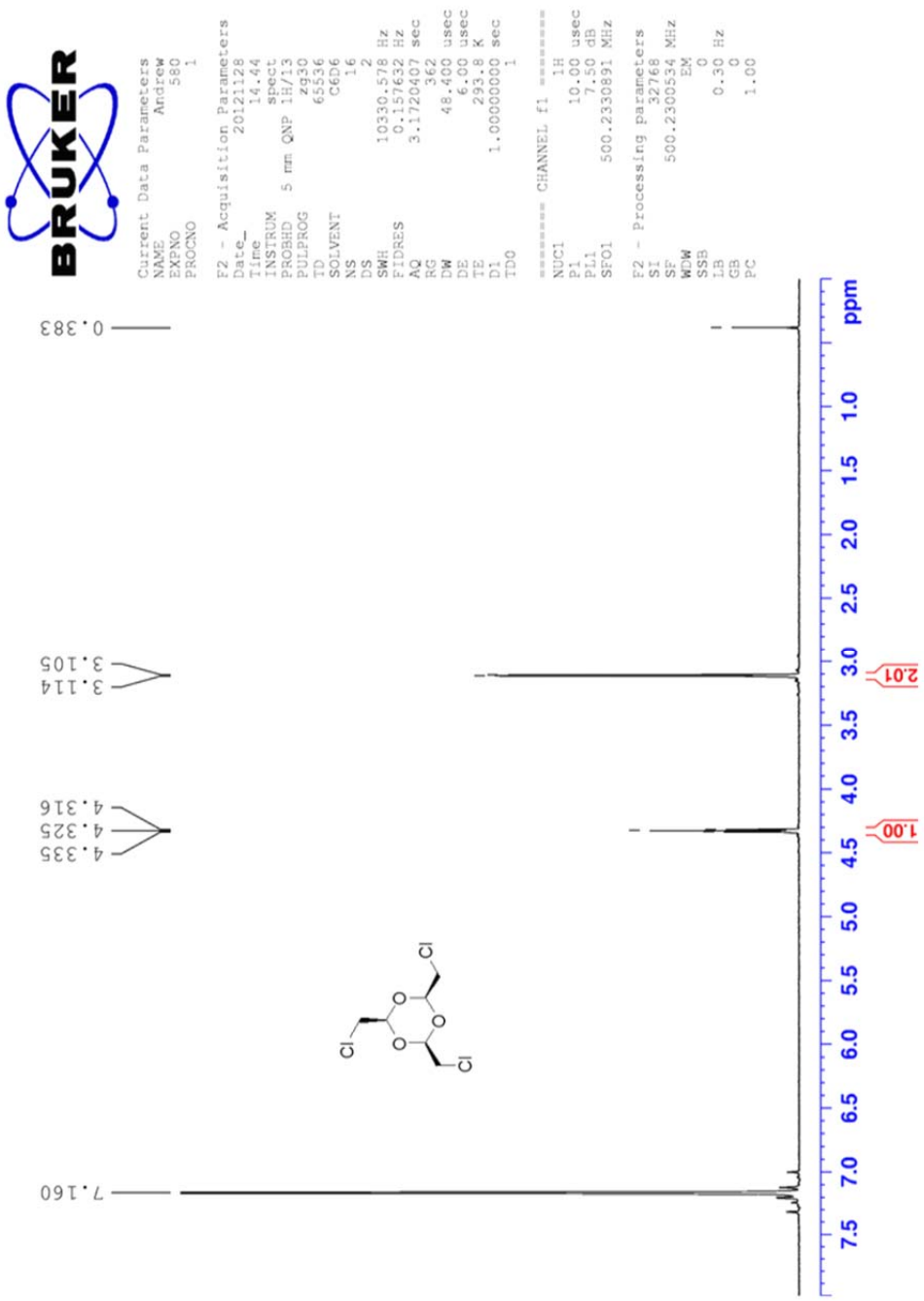

Figure S1. ^{1}H NMR spectrum of compound **3** in d6-benzene

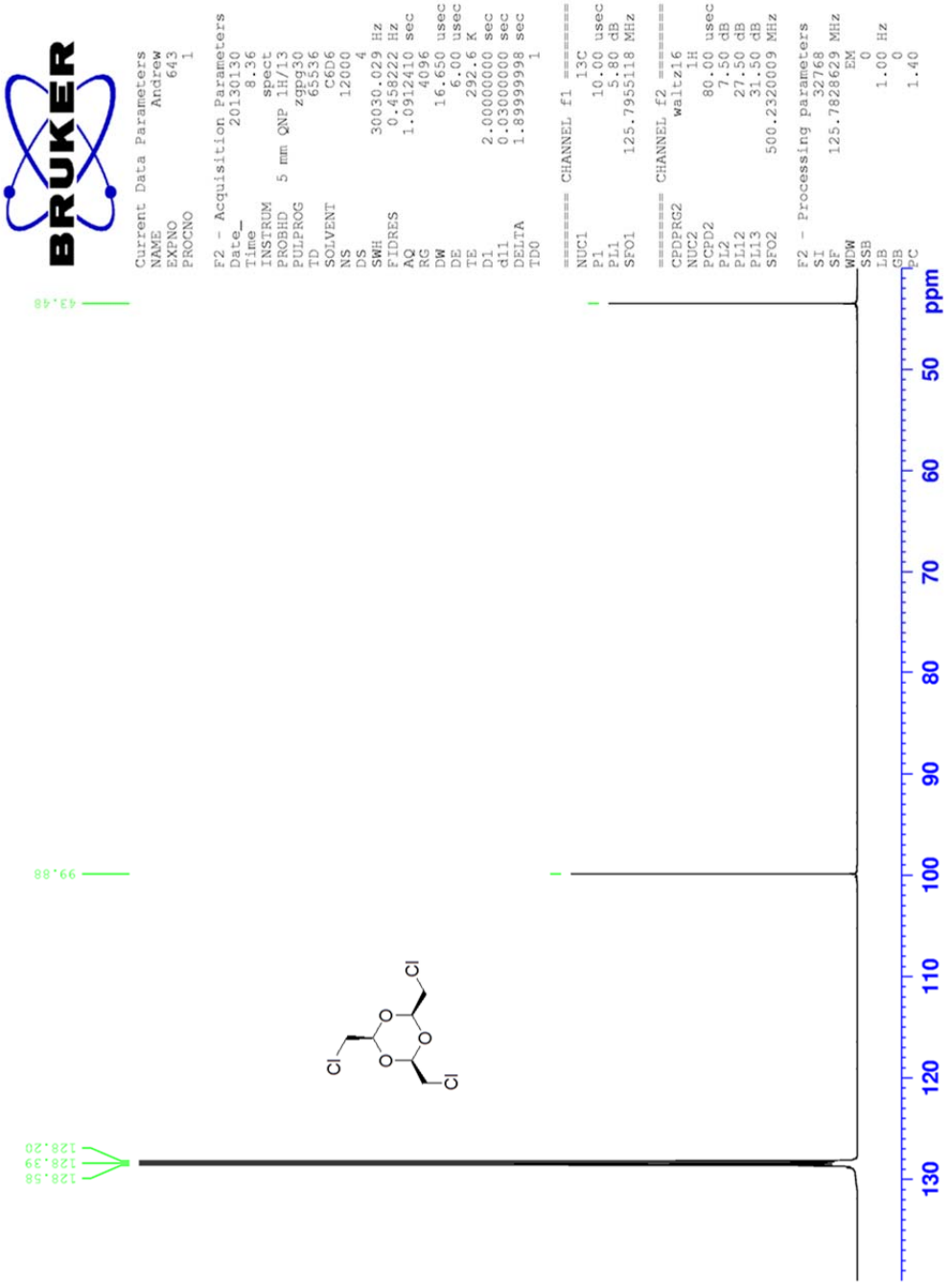

Figure S2. ^{13}C NMR spectrum of compound **3** in d6-benzene

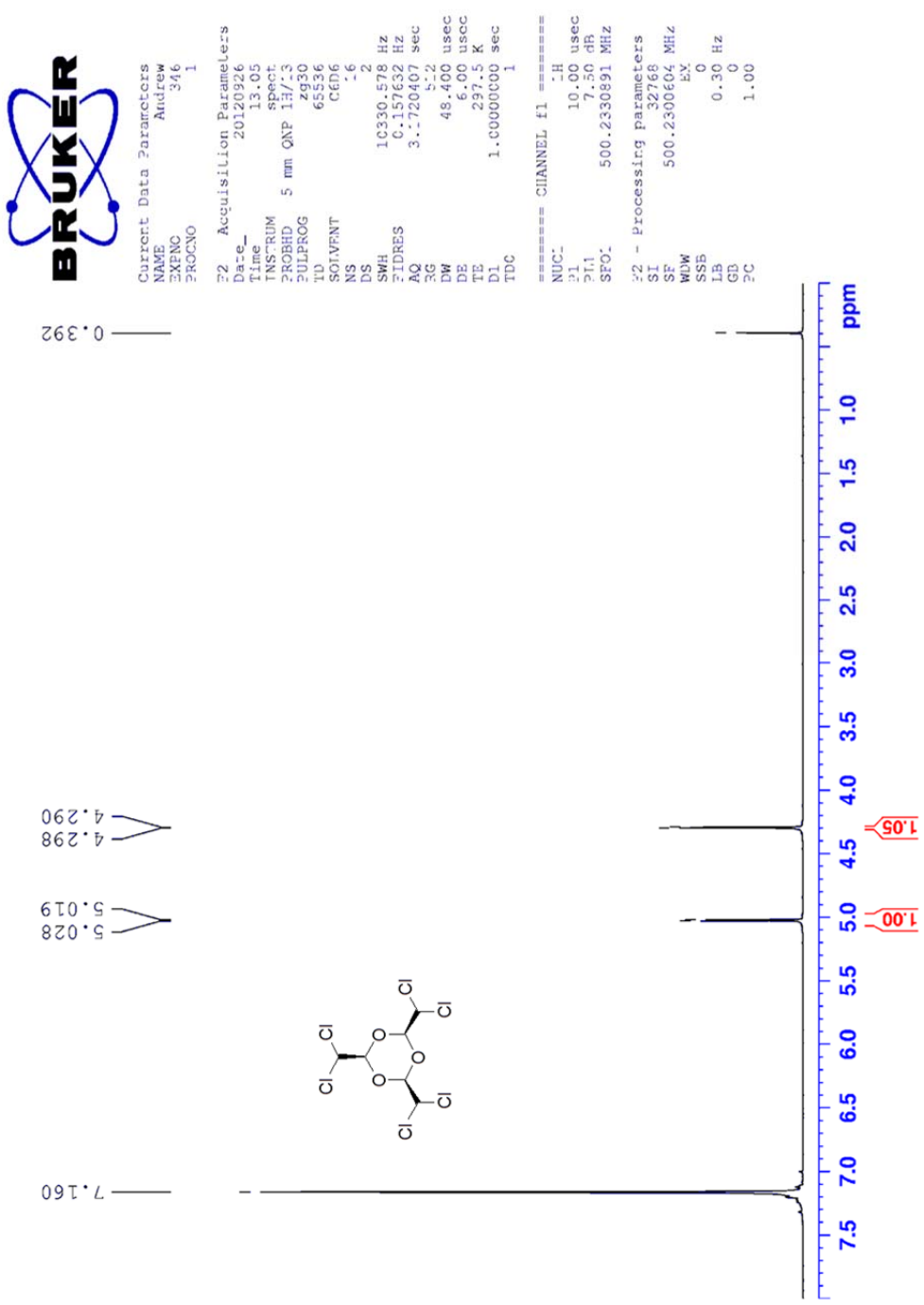

Figure S3. ^{1}H NMR spectrum of compound **4** in d6-benzene

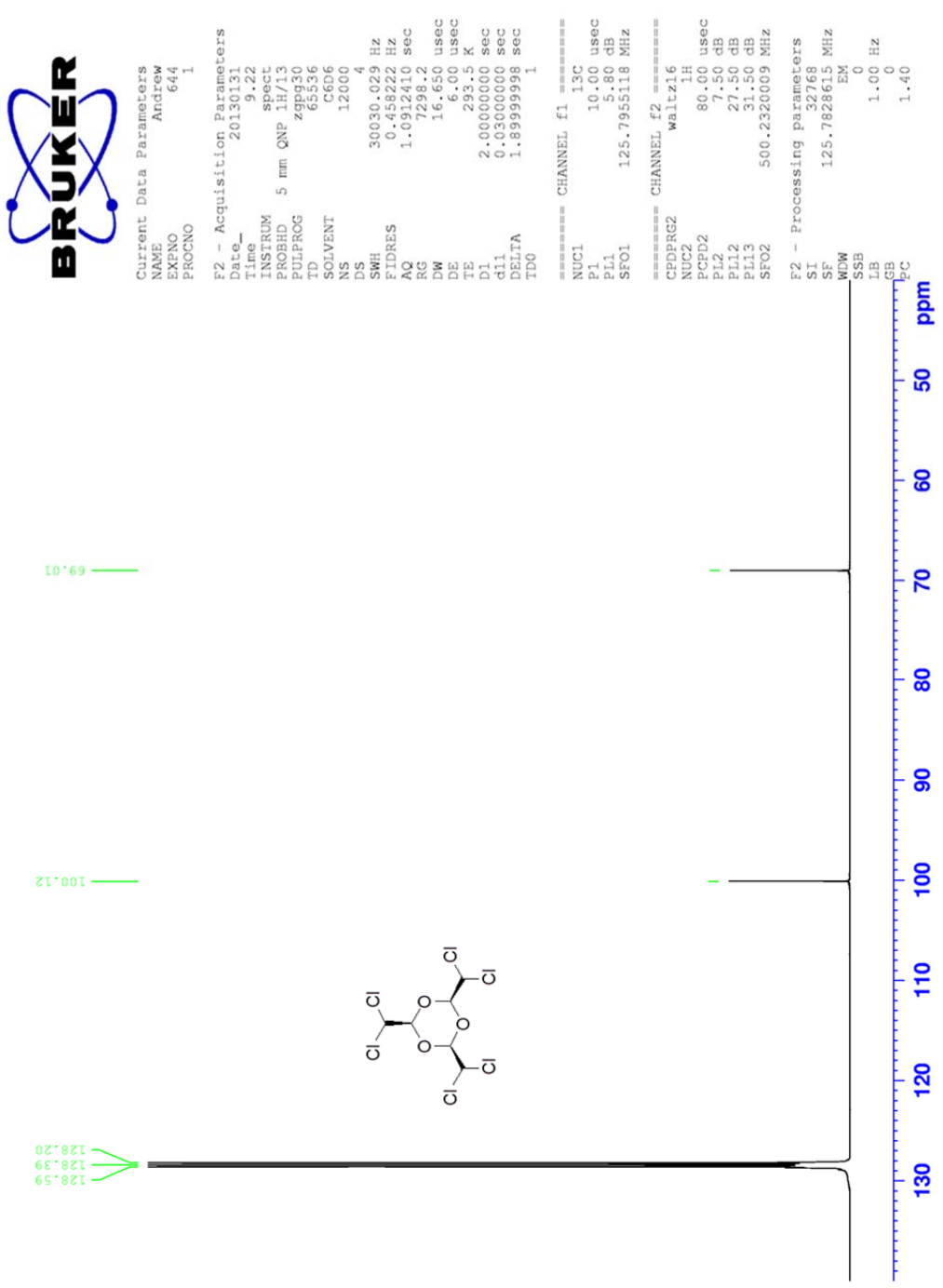

Figure S4. ^{13}C NMR spectrum of compound **4** in d6-benzene

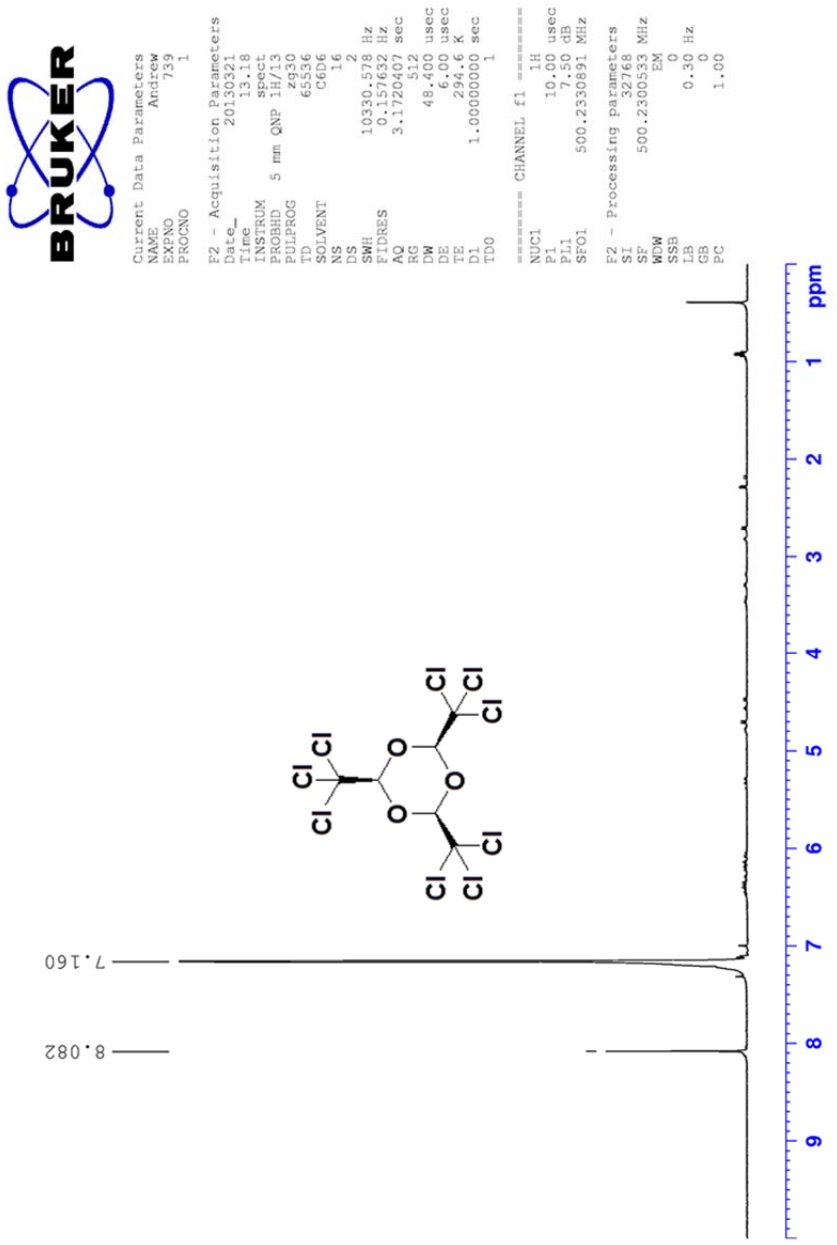

Figure S5. ^{1}H NMR spectrum of compound **5** in d6-benzene

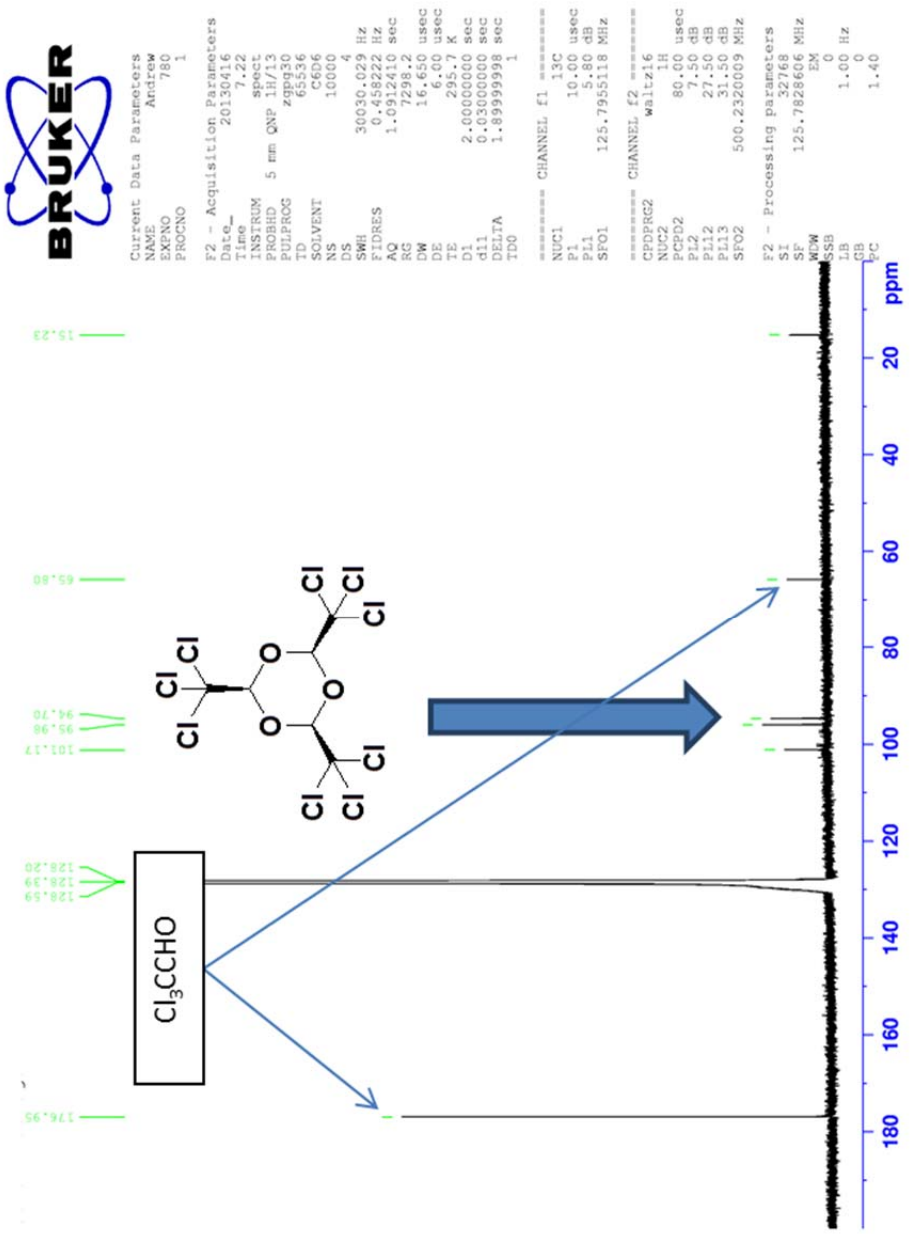

Figure S6. ^{13}C NMR spectrum of compound **5** in d6-benzene. **5** decomposed to chloral while scanning.

3. Methodologies of Calculation

Simulated Annealing Procedure and Determination of Formation Energies for all n

We tried to get all the possible conformations for each multimer (2n-crown-n, where **n** = 2 ~ 6). Here, we applied a simulated annealing procedure to obtain the lowest energy conformations. First 2n-crown-n structures were sketched by the SYBYL8.1[1] software package and minimized by setting all the default parameters. Minimized structures were saved as protein database (pdb) format. These structures were imported in AMBER 12 suite of package.[2] The energy minimization of the structure was performed using the AM1-BCC charge[3] and antechamber program with general amber force field. Amber parameter of the molecule was saved into topology and coordinate files. *In vacuo* steepest descent and conjugate gradient minimization for total 500 steps with 12 Å cutoff were performed, which include first 250 steps of steepest descent and remaining conjugate gradient minimization. After energy minimization the coordinates were used in the next MD simulation process. MD simulation was performed *in vacuo* with Langevin temperature controller coupled with collision frequency of 1.0 (gamma_ln). The output and trajectory coordinates were saved after every 100 steps. Total 500000 steps simulation with disintegration time of 0.002 picosecond (ps) was performed with 12 Å cutoff. Initial and final temperature was set each to 1000 K. Sander program was used for 1 nanosecond. 100 snapshots were saved from this trajectory for further DFT optimization, for each 2n-crown-n ethers. We generated 100 snapshots at 4 ps interval for all the simulated annealing and saved in pdb format. Total 500 snapshots were generated. These structures were converted in Gaussian readable input format. We performed full optimization from these structures with B3LYP/6-311++G** level of theory without any constraint. All the conformers were verified to be at the local minima via frequency calculations.

The number of structures retained is listed as the following.

For n=2, 1 conformer, formation energy = 2.7 kcal/mol.

For n=3, 2 conformers, formation energy = -9.6 kcal/mol.

For n=4, 2 conformers, formation energy = -10.0 kcal/mol.

For n=5, 5 conformers, formation energy = -9.5 kcal/mol.

For n=6, 14 conformers, formation energy = -10.0 kcal/mol.

We have considered mirror image conformers as being the same. The numbers of lowest energy structures obtained are as follows.

Based on the conformers obtained, we chose the lowest energy conformer as the representative structure for each 2n-crown-n structure. the calculated formation energy for each 2n-crown-n is 2.7, -9.6, -10.0, -9.5, and -10.0 kcal/mol for n=2, 3, 4, 5, and 6, respectively.

Relative Stability of Stereoisomers

We tried to get two possible conformations for each compounds shown in Figure below. The all-axial conformer can change to all-equatorial conformer. These structures were fully optimized with B3LYP/6-311++G** level of theory without any constraint. For R=H, both conformers are the same structure. All the conformers were verified to be at the local minima with frequency calculations. As shown in Table below, trioxane itself (**1**) has tetrahedral angle of 109.6˚ (R-C-O). With bulkier substituents, the angle of R-C-O for all-axial conformer becomes larger because of the repulsion between R groups. The average angle for **2**, **3**, and **4** are larger than 112.0˚. Also, the all-axial conformers are significantly less stable than their corresponding all-equatorial ones. For **5** (R=CCl_3), all-axial conformer does not exist, i.e., it spontaneously converts to all-equatorial one, due to very high steric repulsion between R groups. Since the energy differences between all-axial and all-equatorial conformers are very large (more than 4 kcal/mol), the experimentally observed structures should be all equatorial conformers.

The relative energies of axial conformations of **2**, **3** and **4** are

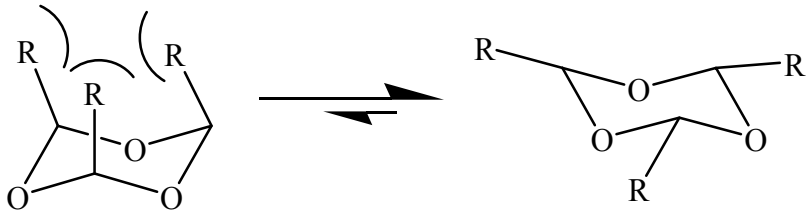

R = H, **(1)**
CH_3, **(2)**
CH_2Cl, **(3)**
$CHCl_2$, **(4)**
CCl_3 **(5)**

Axial Equatorial

R	Relative Energy (kcal/mol)	R-R Distance (Å)	Angle (R-C-O)
(**1**) H	0.00		109.6
(**2**) CH_3	10.91	3.440	114.0
(**3**) CH_2Cl	10.14	3.422	110.8, 115.2
(**4**) $CHCl_2$	14.14	3.527	112.3
(**5**) CCl_3			Non-exist

Gibbs Free Energy and Solvation Energy Calculations

All the calculation were performed with B3LYP/6-31++G** using Gaussian09 package. At the local minimum structures, using the harmonic approximation, Gibbs free energy was calculated with frequency analyses. For solvation energy, PCM (polarizable continuum model) was used. The geometries were again tightly optimized using the dielectric constant of benzene. We performed these calculations to study the nature of the following binding events.

$$\text{Host} + \text{Anion}^- \rightarrow \text{Host}\cdot\text{Anion}^-$$

In the table below, ΔE_{elec} is pure electronic binding energy. ΔE_{BSSEC} is the binding energy after basis set superposition error correction. ΔG_{therm} is the Gibbs binding free energy obtained from Hessian calculations where we confirmed local minimum structures. Then, we performed geometry optimization in benzene solution followed by frequency calculation. Solvation energy calculations (ΔG_{sol}), gave very small binding free energies. For host **1** and **2**, the binding free energy in benzene is positive, and this is consistent with the experimental results. We could not detect any binding with these hosts. For hosts **3**, **4** and **5**, rather small binding energies were obtained. For every calculation results, the trend is very clear: The larger the electron-withdrawing effect of the substitutent is, the stronger the affinity will be.

Table S1. Binding energies between trioxane derivatives and ions (B3LYP/6-31++G**)[a]

Host	Nitrite				Acetate			
	ΔE_{elec}	ΔE_{BSSEC}	ΔG_{therm}	ΔG_{sol}	ΔE_{elec}	ΔE_{BSSEC}	ΔG_{therm}	ΔG_{sol}
1	-13.7	-13.0	-5.1	4.07	-15.2	-14.7	-4.7	5.19
2	-12.6	-11.2	-3.6	4.57	-14.1	-13.4	-3.1	5.14
3	-26.6	-24.6	-16.0	-3.48	-30.6	-26.8	-14.6	-2.64
4	-27.8	-26.5	-17.5	-3.59	-31.0	-29.4	-18.1	-4.56
5	-29.4	-28.0	-18.7	-4.43	-32.9	-31.4	-19.8	-5.52

[a] ΔE_{elec}: pure electronic binding energy; ΔE_{BSSEC}, binding energy after BSSEC. ΔG_{therm}: Gibbs binding free energy; ΔG_{sol}: binding energy using the structure optimized in benzene with thermal correction. Units are in kcal/mol.

For Halide binding, to compare with experimental results, we performed solvation energy correction with acetonitrile solvent. We fully optimized the complex structures in gas phase, followed by frequency calculation; basis set superposition error correction, and solvation energy calculations. The overall trends are very similar to those of acetate and nitrite in benzene. Although binding affinities are low, it is clear that the absolute magnitude of halide bining affinity depends on the electronic nature of substituent.

Table S2. Binding energies between trioxane derivatives and Halides in Acetonitrile

Host	F^-				Cl^-			
	ΔE_{elec}	ΔE_{BSSEC}	ΔG_{therm}	ΔG_{sol}	ΔE_{elec}	ΔE_{BSSEC}	ΔG_{therm}	ΔG_{sol}
1	-24.9	-23.3	-24.1	1.7	-13.2	-13.0	-15.2	-0.9
2	-23.8	-22.1	-23.0	2.6	-12.1	-11.8	-14.2	-0.6
3	-34.2	-32.3	-33.1	-0.4	-18.8	-18.5	-20.4	-1.0
4	-45.8	-43.8	-44.5	-3.6	-27.5	-27.0	-28.7	-2.6
5	-49.2	-47.1	-47.9	-5.7	-29.2	-28.7	-30.4	-3.5

[a] E_{elec}, pure electronic binding energy; E_{BSSEC}, binding energy after BSSEC. G_{therm}, Gibbs binding free energy; G_{sol}, binding energy using the structure optimized in gas phase with thermal correction. Solvation effects were considered using these geometries. Units are in kcal/mol. (B3LYP/6-31++G**)[a]

Table S2. (Continued)

Host	Br^-				I^- [b]			
	ΔE_{elec}	ΔE_{BSSEC}	ΔG_{therm}	ΔG_{sol}	ΔE_{elec}	ΔE_{BSSEC}	ΔG_{therm}	ΔG_{sol}
1	-16.4	-10.8	-13.5	-0.9	-14.6	-9.8	-12.8	0.0
2	-17.1	-9.6	-12.2	-0.2	-13.2	-8.1	-11.3	0.4
3	-24.2	-15.5	-17.5	-0.4	-20.1	-14.3	-17.6	-1.5
4	-33.7	-23.4	-25.2	-1.7	-29.9	-23.5	-26.2	-2.0
5	-36.2	-24.7	-26.6	-2.5	-32.1	-25.4	-28.5	-3.0

[b] 3-21G* Basis set was used for Iodide.

4. Binding Constant Determination

All NMR spectroscopic titration experiments were performed as follows: d6-benzene solution of host compound (4.0 mM) was titrated by d6-benzene solution of $TBANO_2$ (100 mM) or TBAOAc (50 mM), until the chemical shift of protons on host compound became stable (saturation, $\boldsymbol{\delta_{sat}}$). $\boldsymbol{\delta_{sat}}$ is a kind of observed chemical shift ($\boldsymbol{\delta_{obs}}$) when $\mathbf{[G] \approx [G_0]}$. Then, 8.00 mM d6-benzene solution of both host and guest were prepared, and mixed by the volume ratio of 1:9, 2:8, to 9:1. Binding constant (**K**) and proton chemical shifts of host-guest complex ($\boldsymbol{\delta_{fin}}$) were extrapolated from correlation formula $\boldsymbol{\delta_{rel} = (\delta_{obs} - \delta_{ini})/(\delta_{fin} - \delta_{ini}) = [HG]/[H_0]}$ and thermodynamic formula $\mathbf{K = [HG]/[([H_0]-[HG])([G_0]-[HG])]}$, in which $\boldsymbol{\delta_{ini}}$ refers to chemical shift of specific protons of the pure host. At the same time, the corresponding Job plot was plotted. Two parallel experiments were conducted for one host-guest combination, and the average results were calculated by applying the arithmetic averages of observed chemical shifts ($\boldsymbol{\delta_{obs}}$).

NMR titration of compound 3 and TBAOAc:

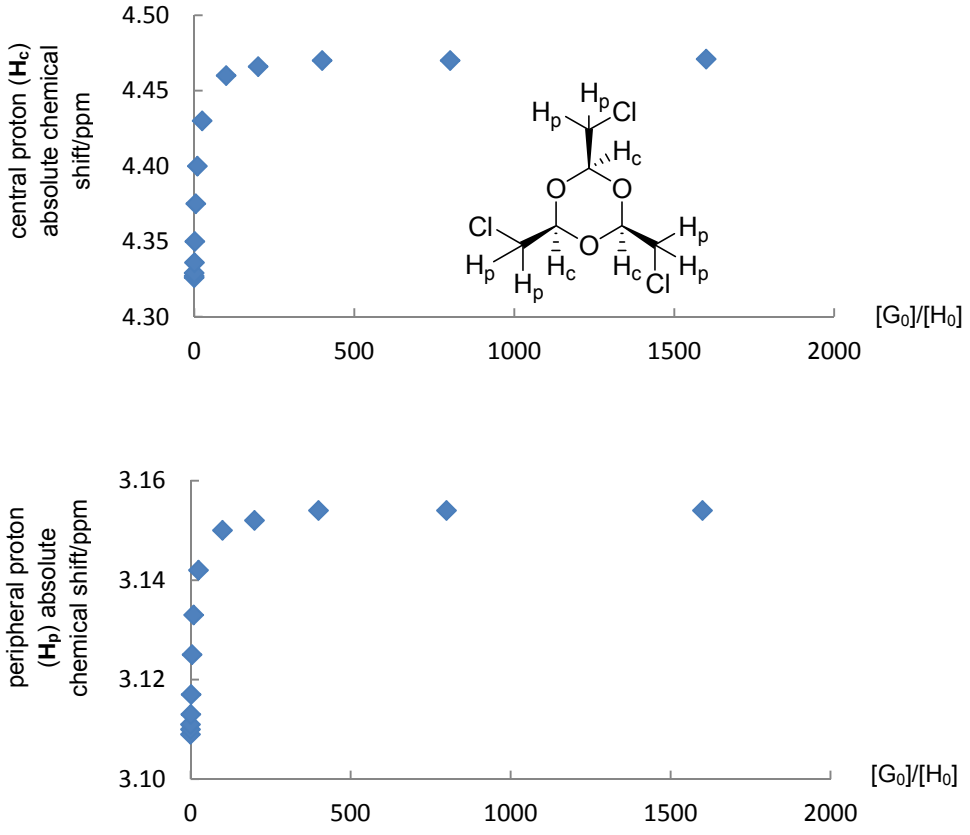

Figure S7. ^{1}HNMR chemical shifts of **3** and TBAOAc interaction. 4.00 mM of **3** was titrated by 50.00 mM of TBAOAc in d6-benzene.

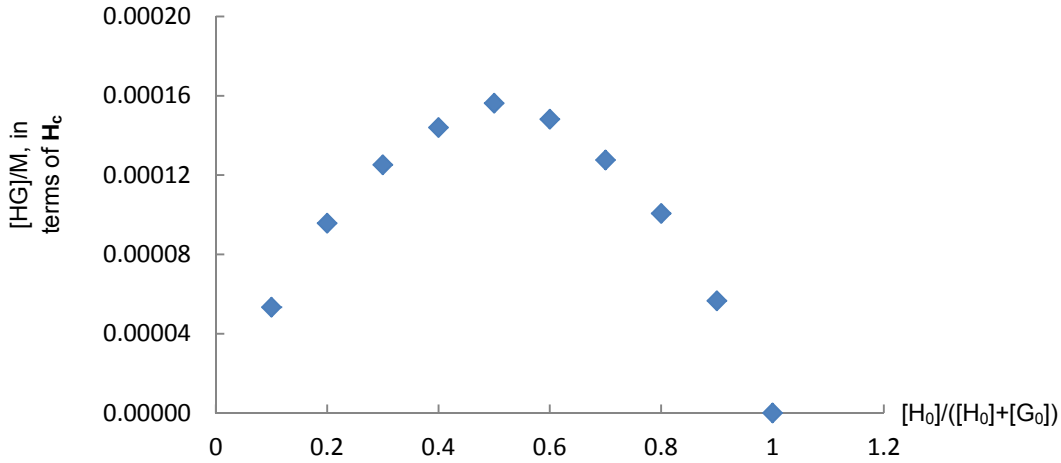

Figure S8. Job Plot of **3** and TBAOAc interaction in d6-benzene. $[H_0]+[G_0]$ = 8.00 mM.

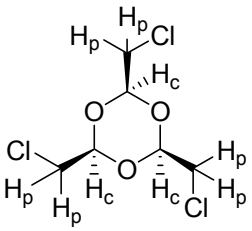

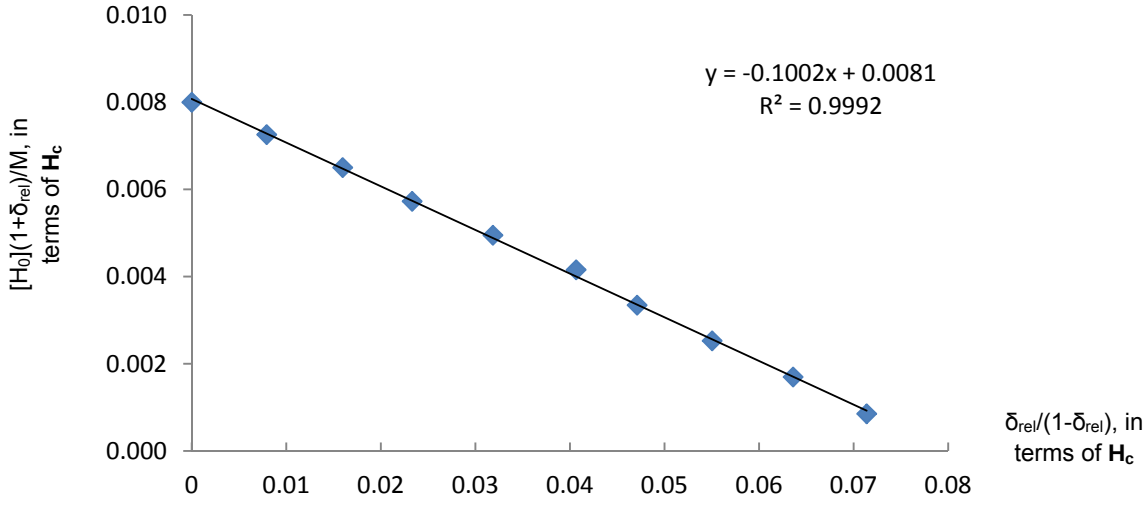

Figure S9. Relationship between $\delta_{rel}/(1-\delta_{rel})$ and $[H_0](1+\delta_{rel})$ for **3** and TBAOAc interaction in d6-benzene. $[H_0]+[G_0]$ = 8.00 mM. The slope of the fitted line is -1/K, and the intercept is $[H_0]+[G_0]$.

NMR titration of compound 4 and TBAOAc:

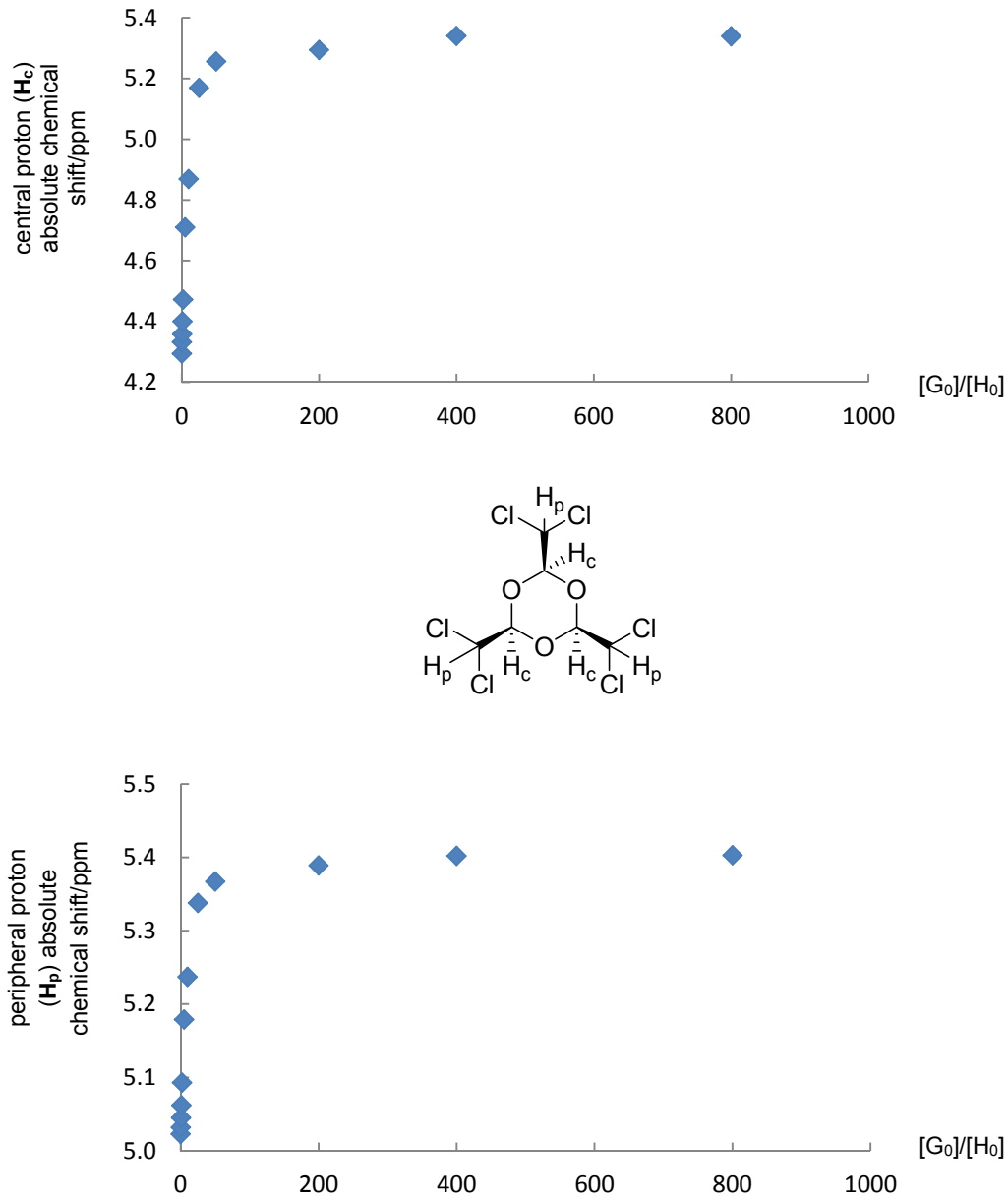

Figure S10. [1]HNMR chemical shifts of **4** and TBAOAc interaction. 4.00 mM of **4** was titrated by 50.00 mM of TBAOAc in d6-benzene.

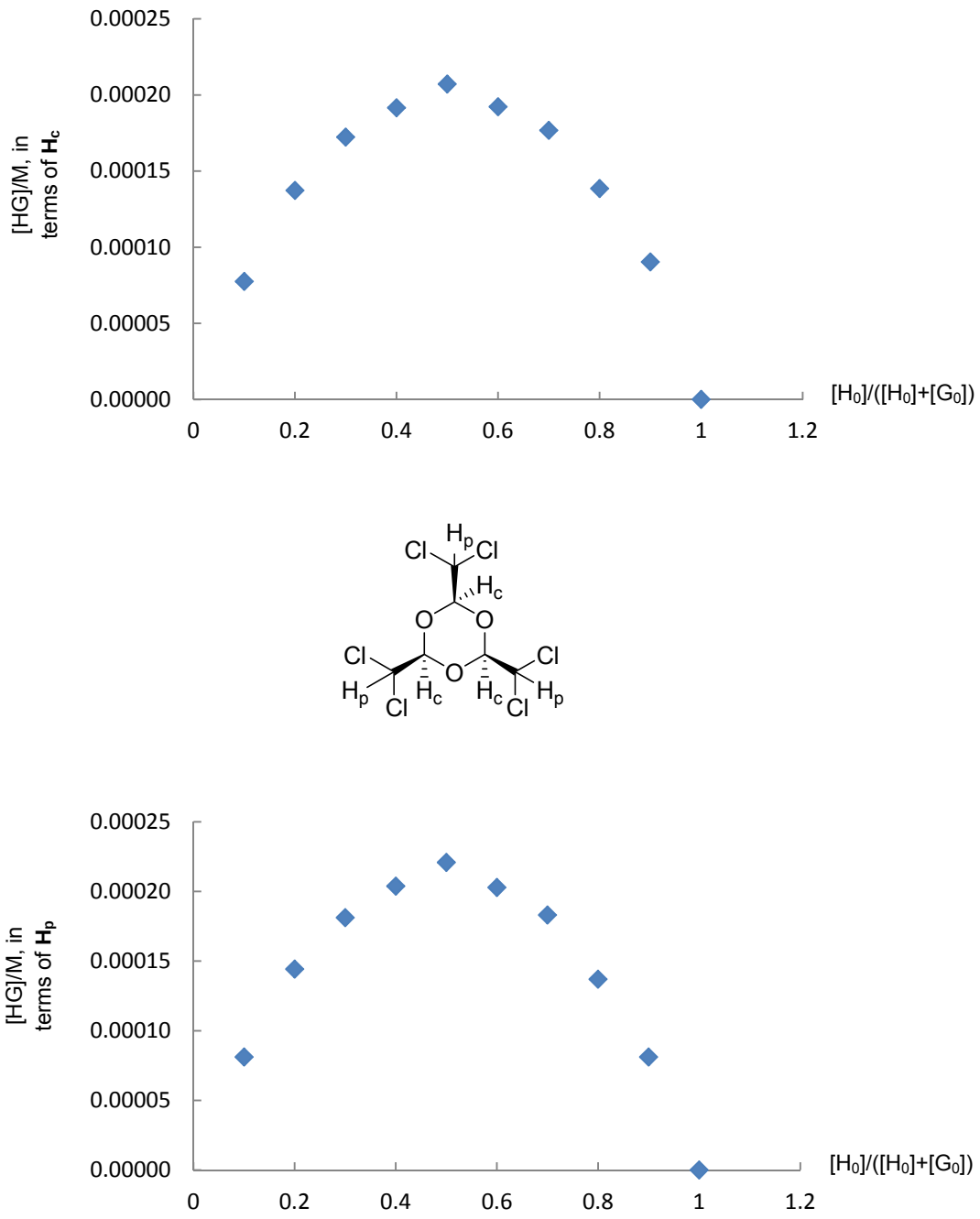

Figure S11. Job Plots of **4** and TBAOAc interaction in d6-benzene. $[H_0]+[G_0]$ = 8.00 mM.

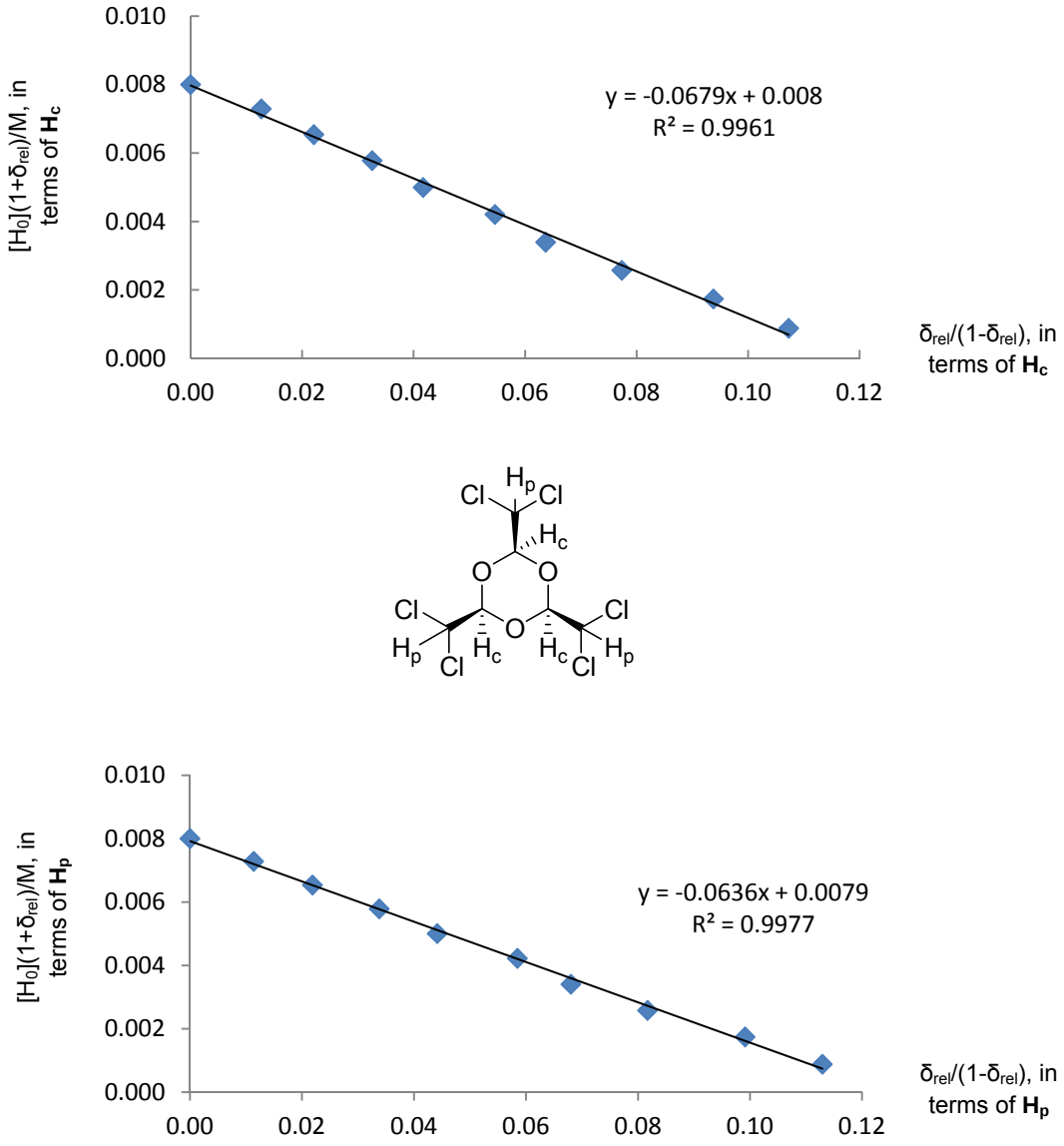

Figure S12. Relationship between $\delta_{rel}/(1-\delta_{rel})$ and $[H_0](1+\delta_{rel})$ for **4** and TBAOAc interaction in d6-benzene. $[H_0]+[G_0]$ = 8.00 mM. The slope of the fitted line is -1/K, and the intercept is $[H_0]+[G_0]$.

NMR titration of compound 3 and $TBANO_2$:

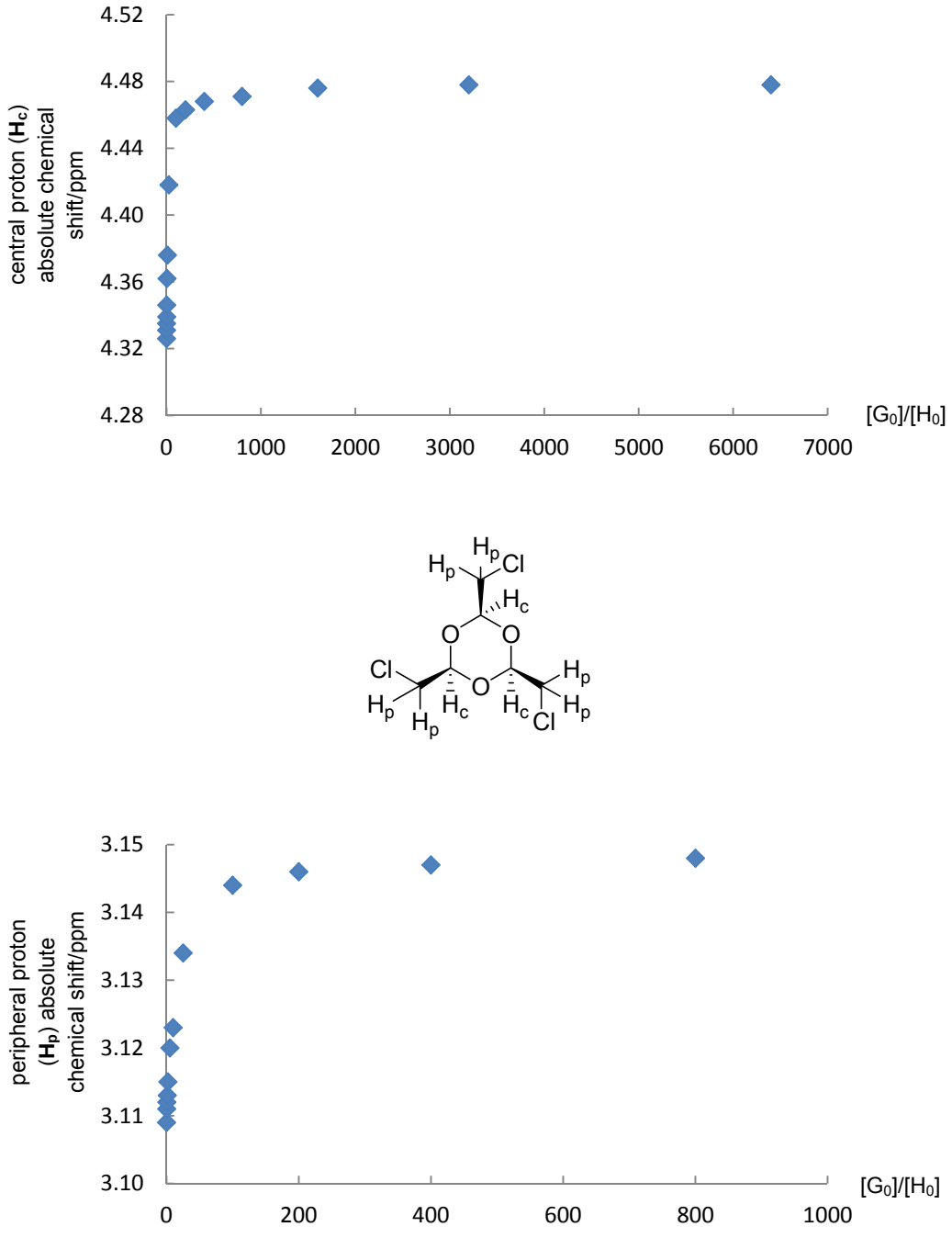

Figure S13. ^{1}HNMR chemical shifts of **3** and $TBANO_2$ interaction. 4.00 mM of **3** was titrated by 100.00 mM of $TBANO_2$ in d6-benzene. In case of $\mathbf{H_p}$, when $[G_0]/[H_0]$ exceeds 800, the peak of $\mathbf{H_p}$ will overlap with one peak of tetrabutylammonium cation.

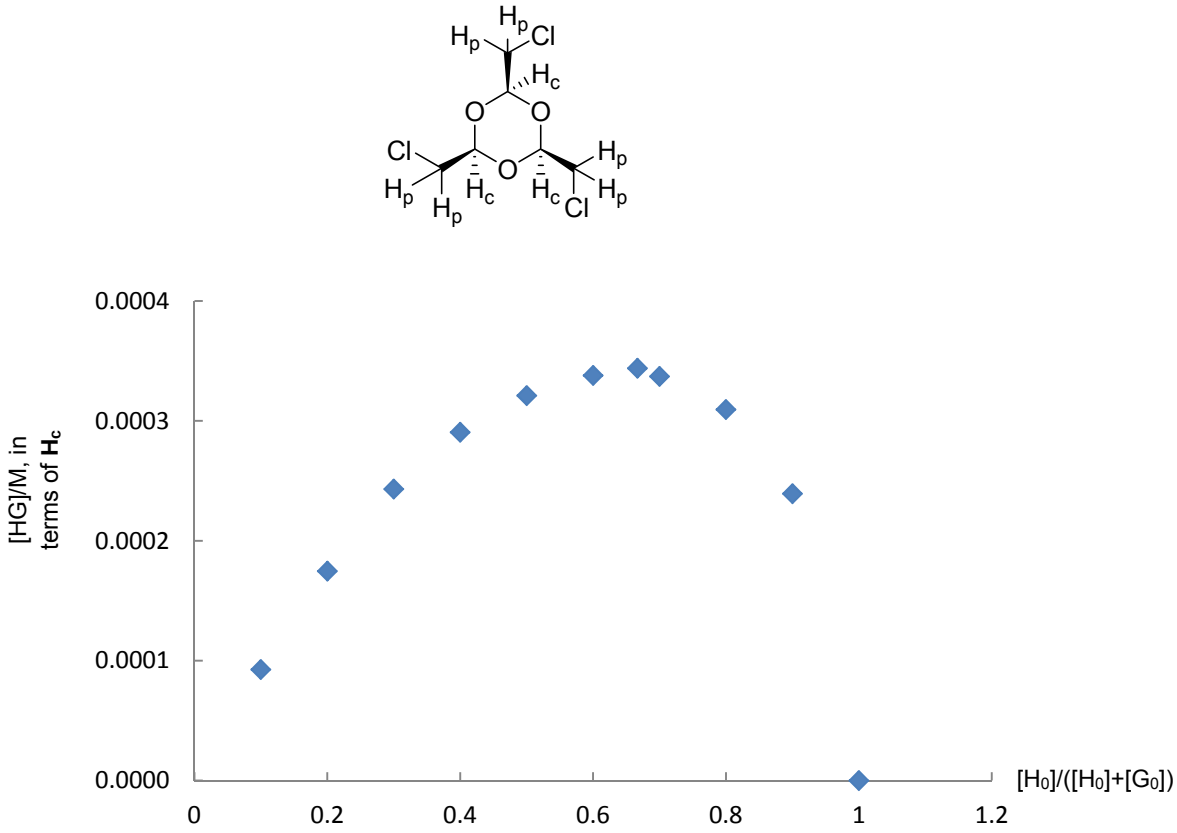

Figure S14. Job Plot of **3** and $TBANO_2$ interaction in d6-benzene. $[H_0]+[G_0]$ = 8.00 mM.

NMR titration of compound 4 and $TBANO_2$:

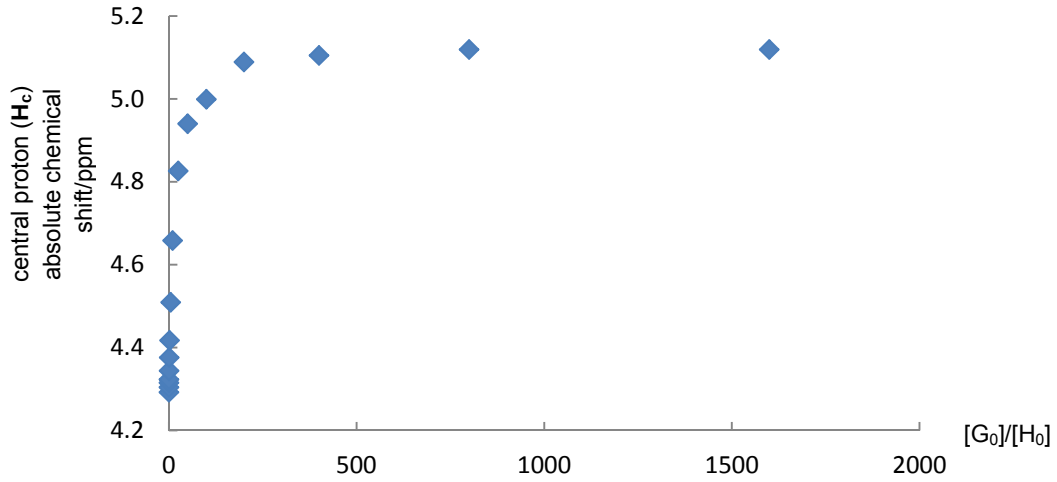

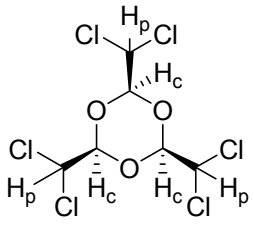

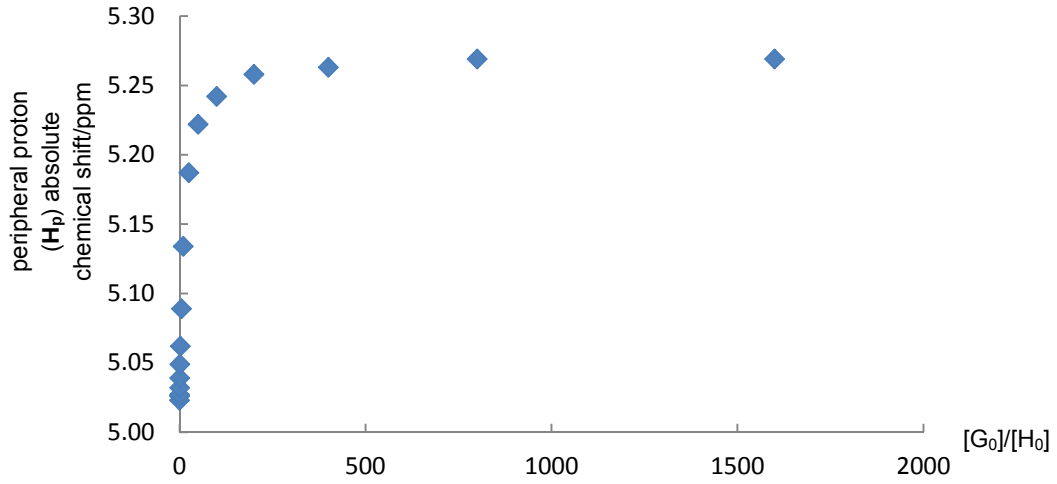

Figure S15. ^{1}HNMR chemical shifts of **4** and $TBANO_2$ interaction. 4.00 mM of **4** was titrated by 100.00 mM of TBAOAc in d6-benzene.

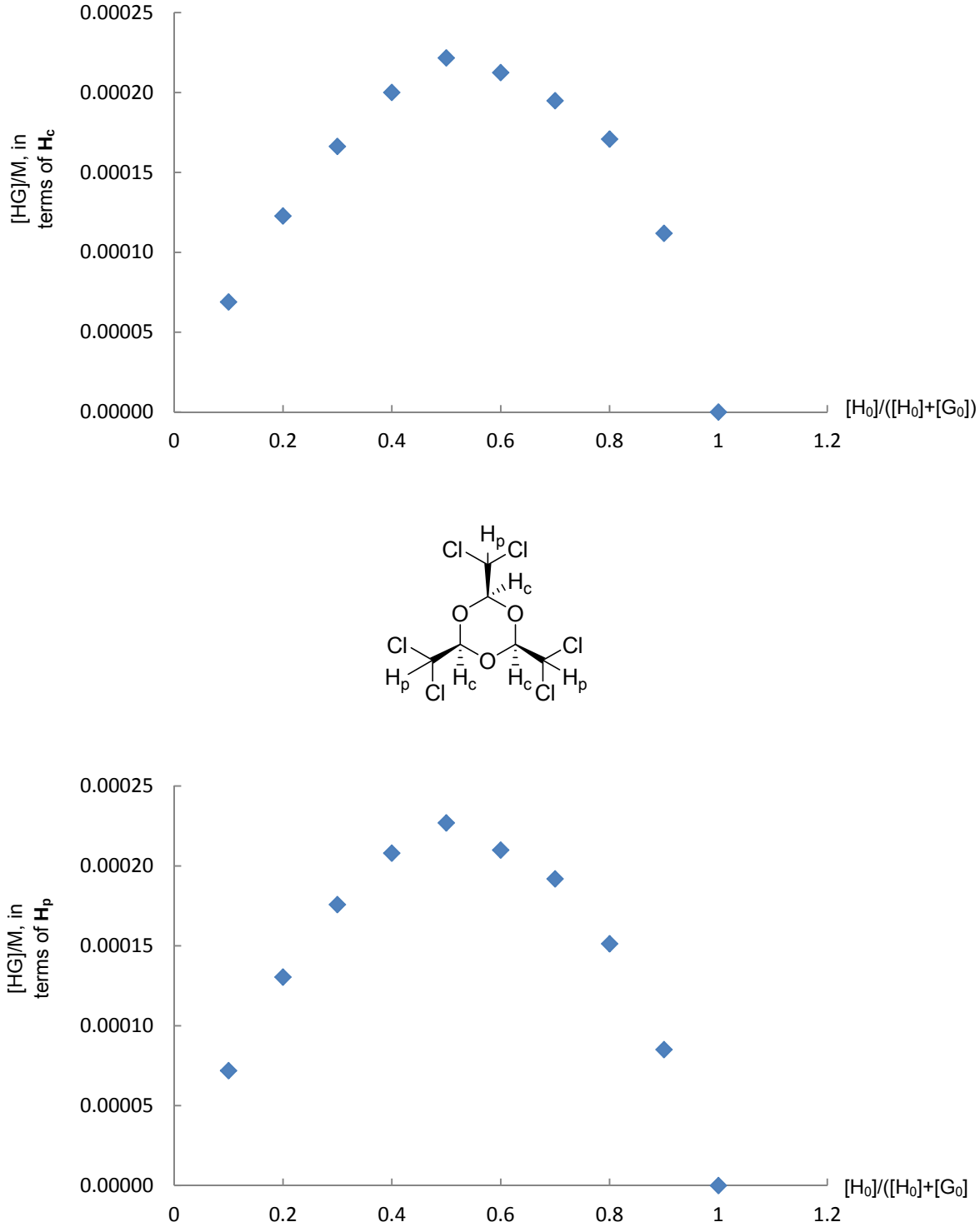

Figure S16. Job Plots of **4** and $TBANO_2$ interaction in d6-benzene. $[H_0]+[G_0]$ = 8.00 mM.

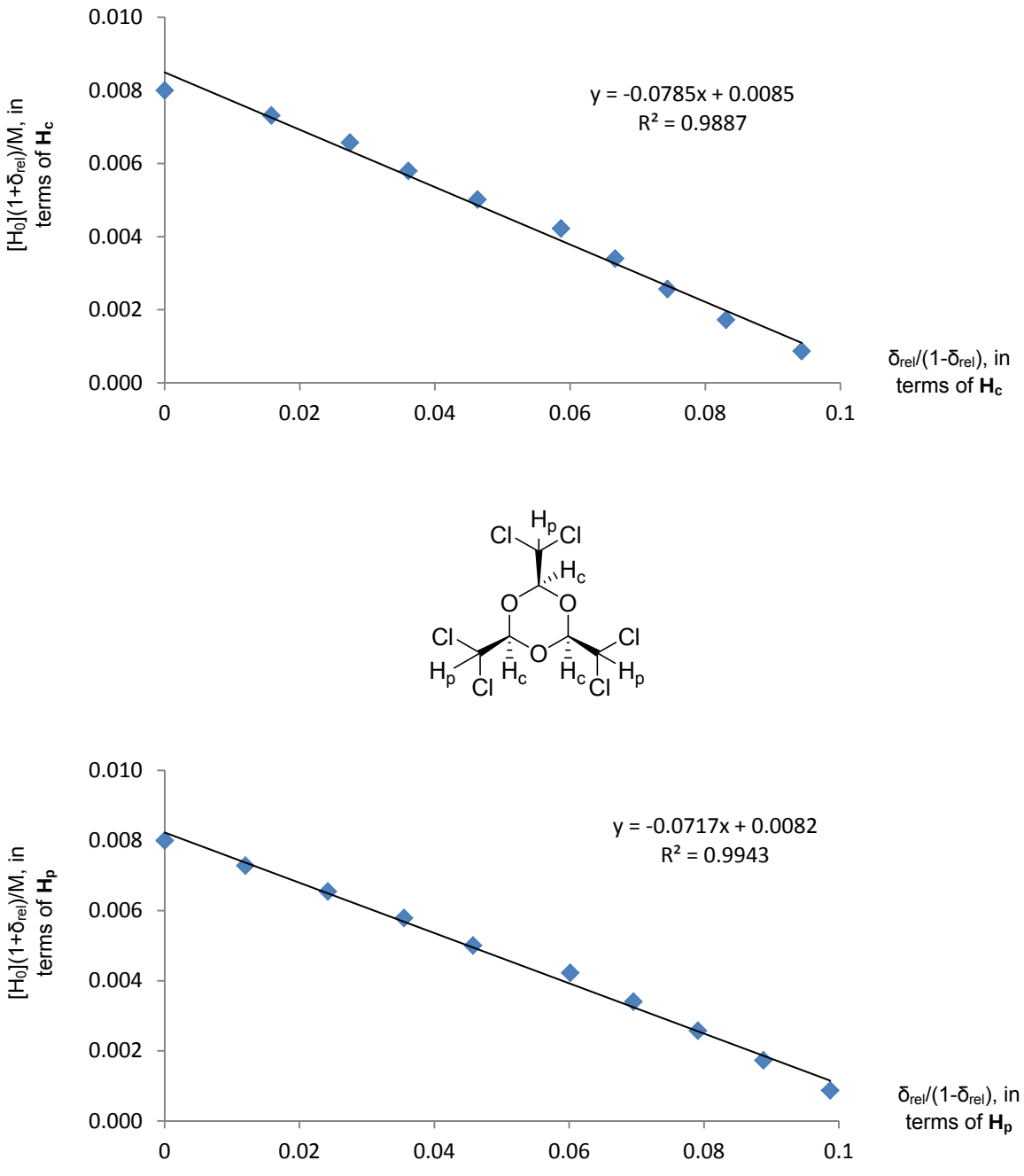

Figure S17. Relationship between $\delta_{rel}/(1-\delta_{rel})$ and $[H_0](1+\delta_{rel})$ for **4** and $TBANO_2$ interaction in d6-benzene. $[H_0]+[G_0]$ = 8.00 mM. The slope of the fitted line is -1/K, and the intercept is $[H_0]+[G_0]$.

NMR titration of compound 3 and TBACl:

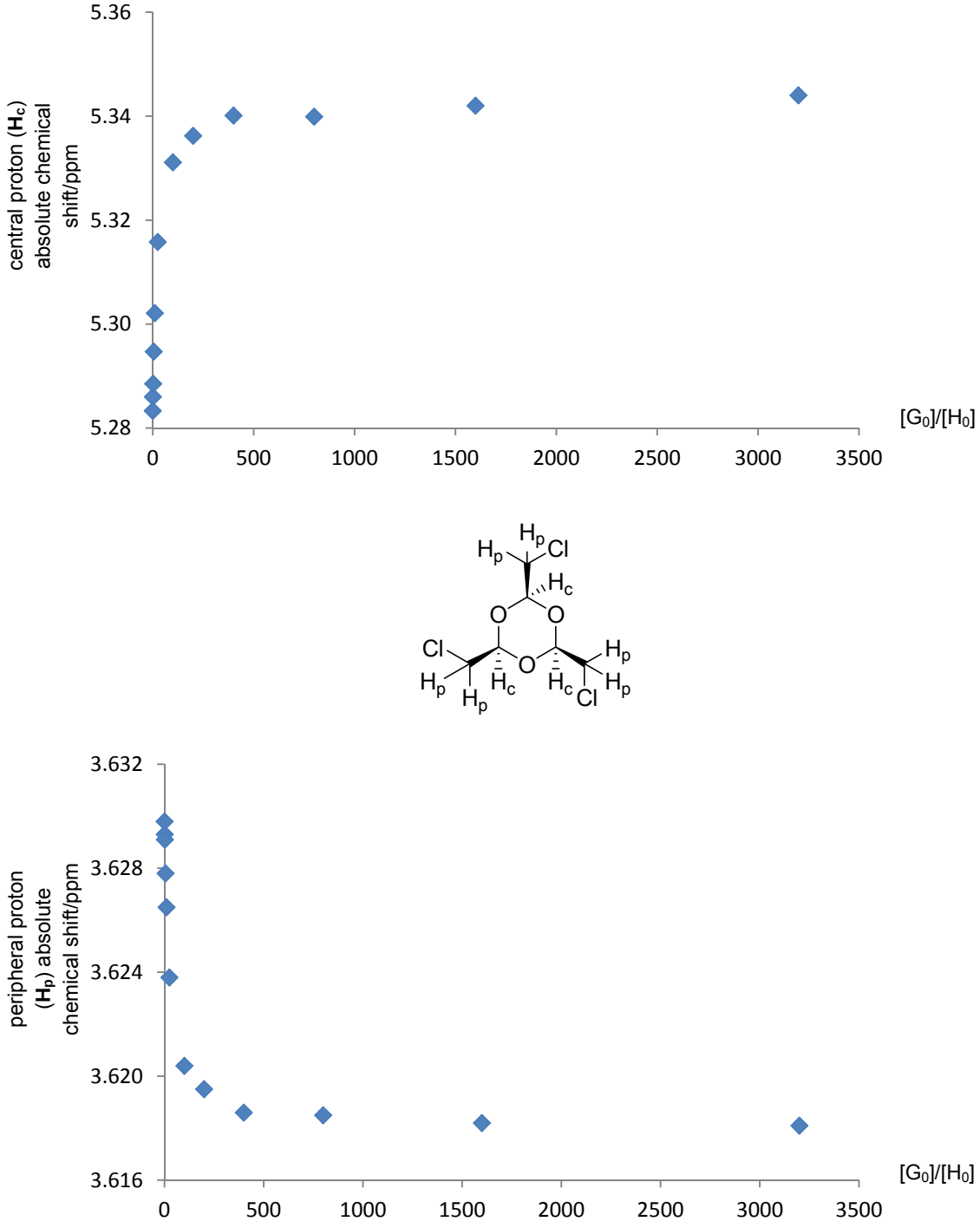

Figure S18. [1]HNMR chemical shifts of **3** and TBACl interaction. 4.00 mM of **3** was titrated by 100.00 mM of TBACl in d3-acetonitrile.

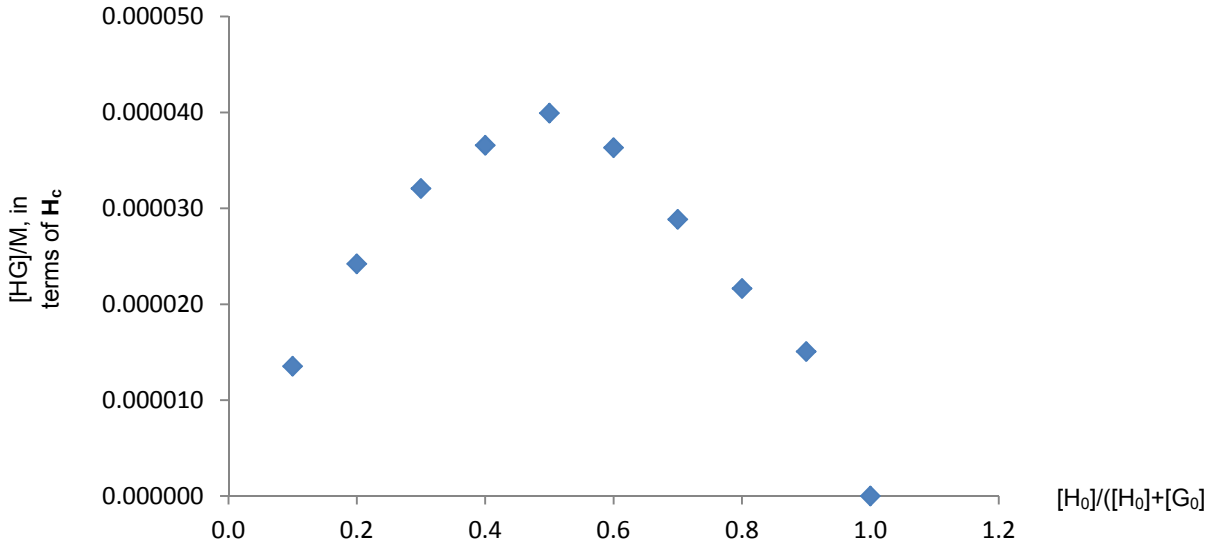

Figure S19. Job Plot of **3** and TBACl interaction in d3-acetonitrile. $[H_0]+[G_0]$ = 8.00 mM.

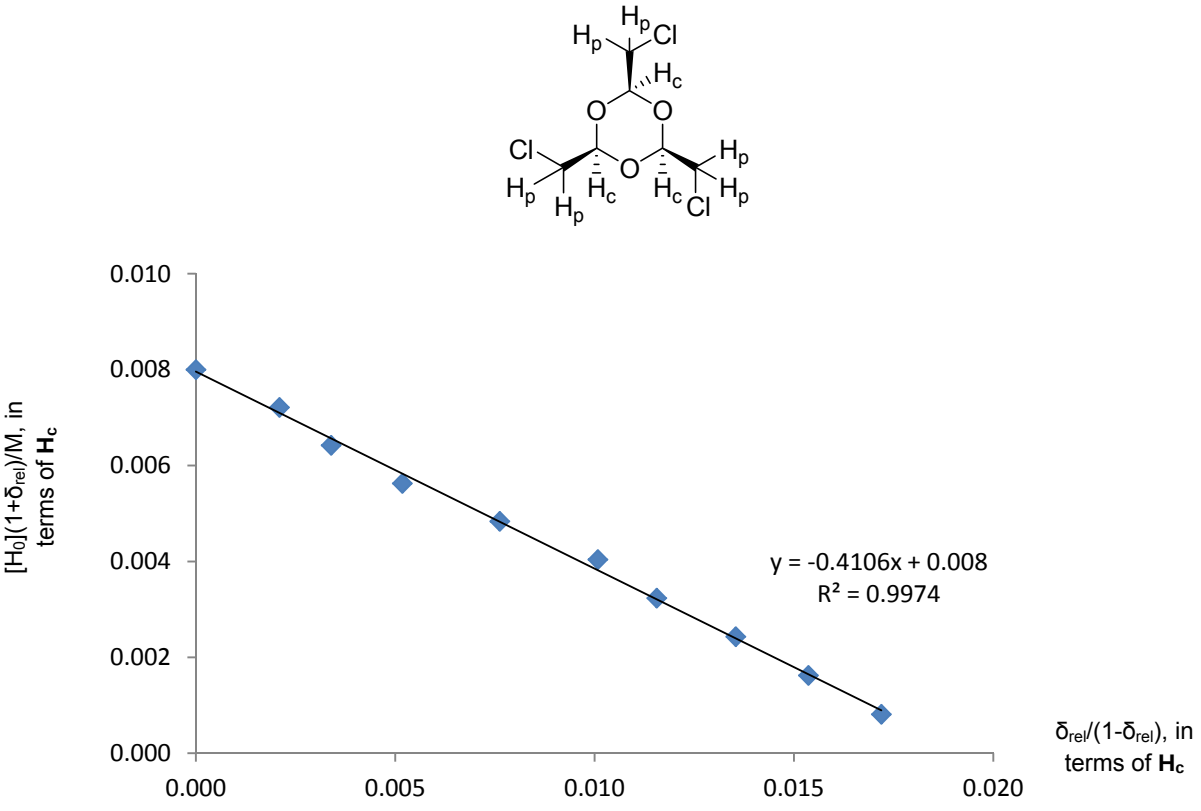

Figure S20. Relationship between $\boldsymbol{\delta_{rel}/(1-\delta_{rel})}$ and $\boldsymbol{[H_0](1+\delta_{rel})}$ for **3** and TBACl interaction in d3-acetonitrile. $[H_0]+[G_0]$ = 8.00 mM. The slope of the fitted line is -1/K, and the intercept is $[H_0]+[G_0]$.

NMR titration of compound 3 and TBABr:

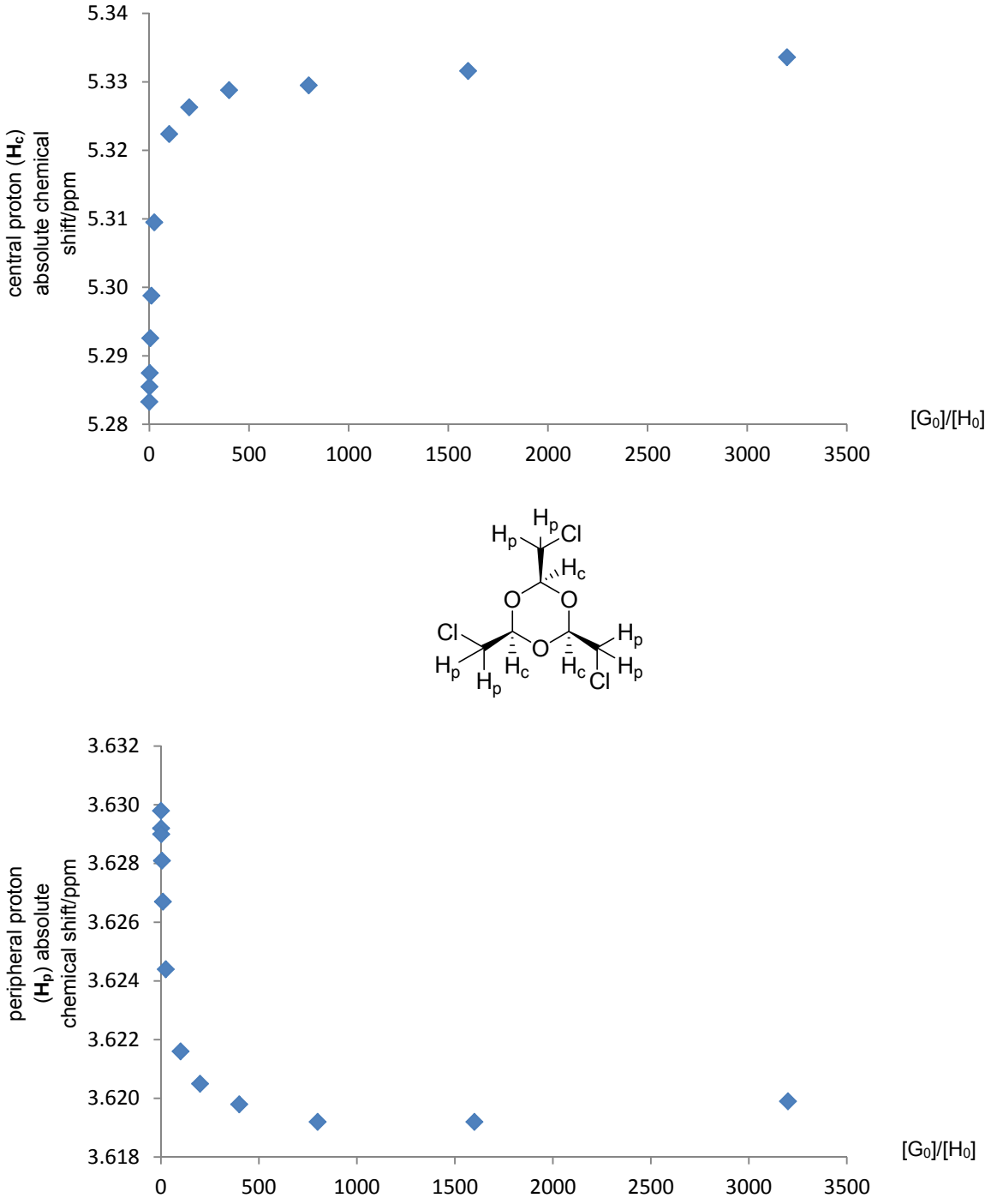

Figure S21. [1]HNMR chemical shifts of **3** and TBABr interaction. 4.00 mM of **3** was titrated by 100.00 mM of TBABr in d3-acetonitrile.

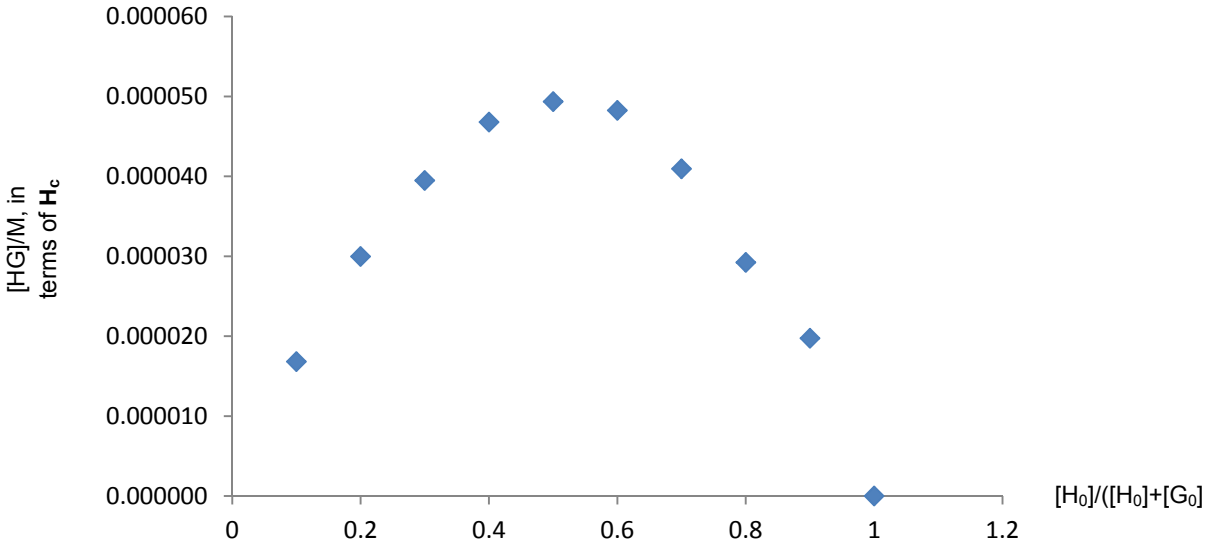

Figure S22. Job Plot of **3** and TBABr interaction in d3-acetonitrile. $[H_0]+[G_0]$ = 8.00 mM.

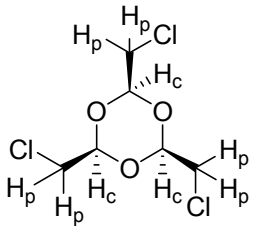

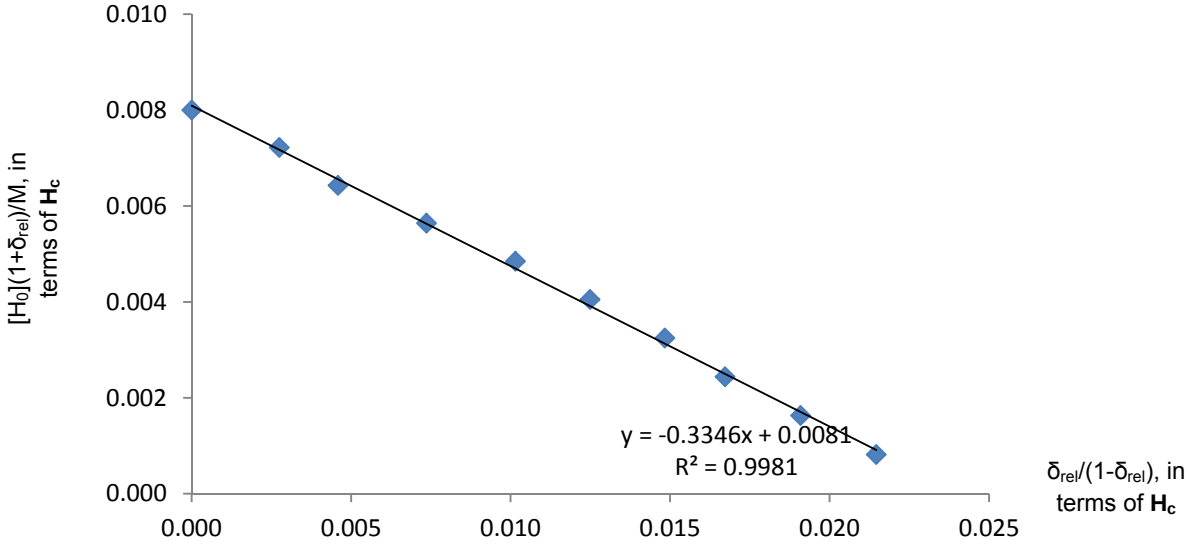

Figure S23. Relationship between $\boldsymbol{\delta_{rel}/(1-\delta_{rel})}$ and $\boldsymbol{[H_0](1+\delta_{rel})}$ for **3** and TBABr interaction in d3-acetonitrile. $[H_0]+[G_0]$ = 8.00 mM. The slope of the fitted line is -1/K, and the intercept is $[H_0]+[G_0]$.

NMR titration of compound 3 and TBAI:

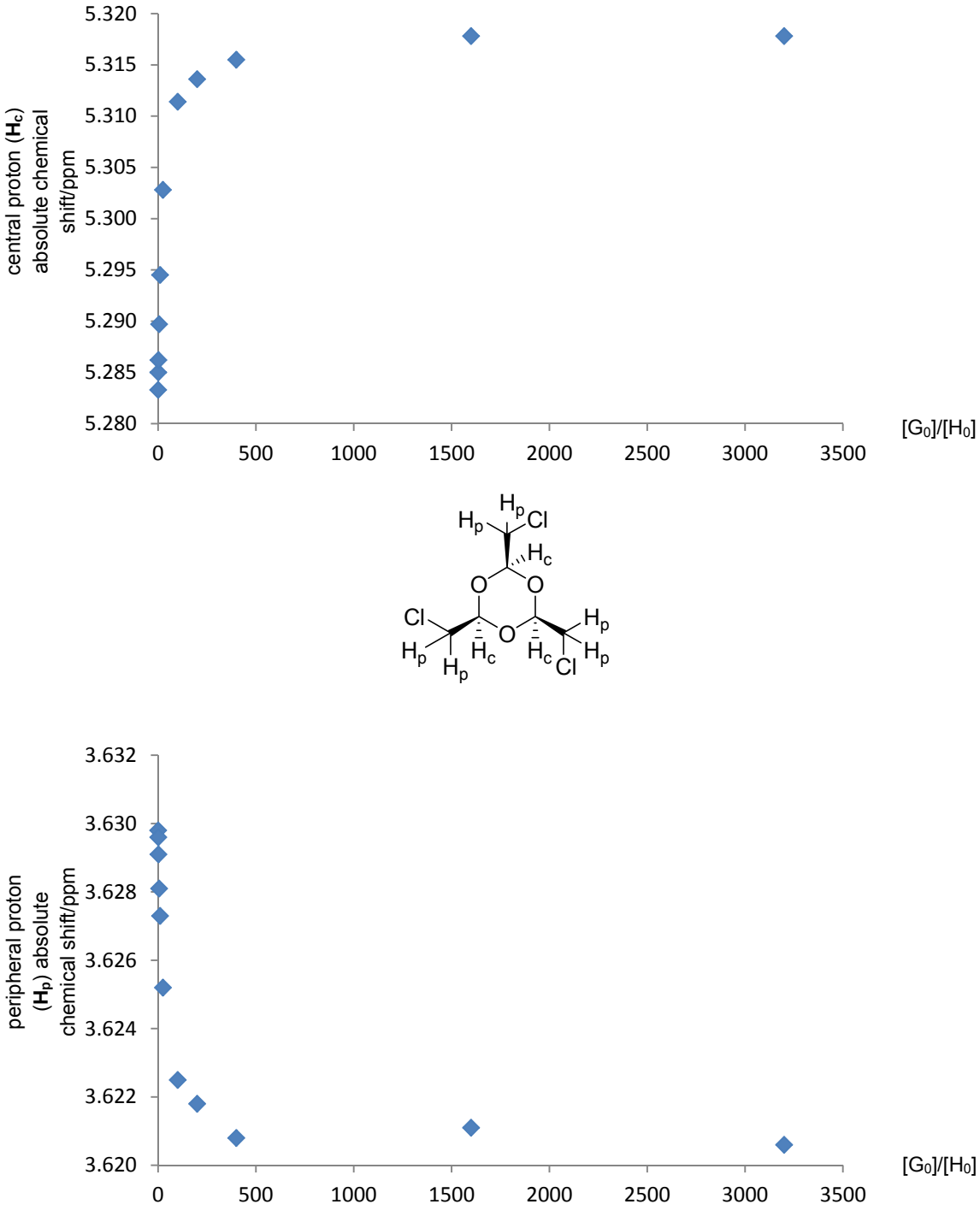

Figure S24. [1]HNMR chemical shifts of **3** and TBAI interaction. 4.00 mM of **3** was titrated by 100.00 mM of TBAI in d3-acetonitrile.

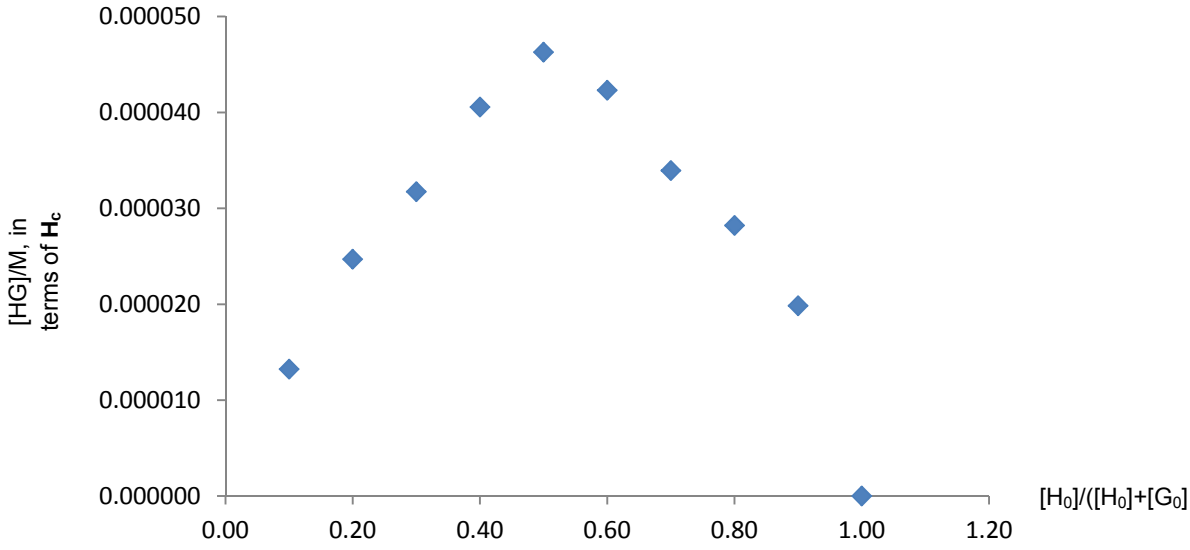

Figure S25. Job Plot of **3** and TBAI interaction in d3-acetonitrile. $[H_0]+[G_0]$ = 8.00 mM.

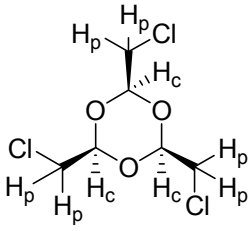

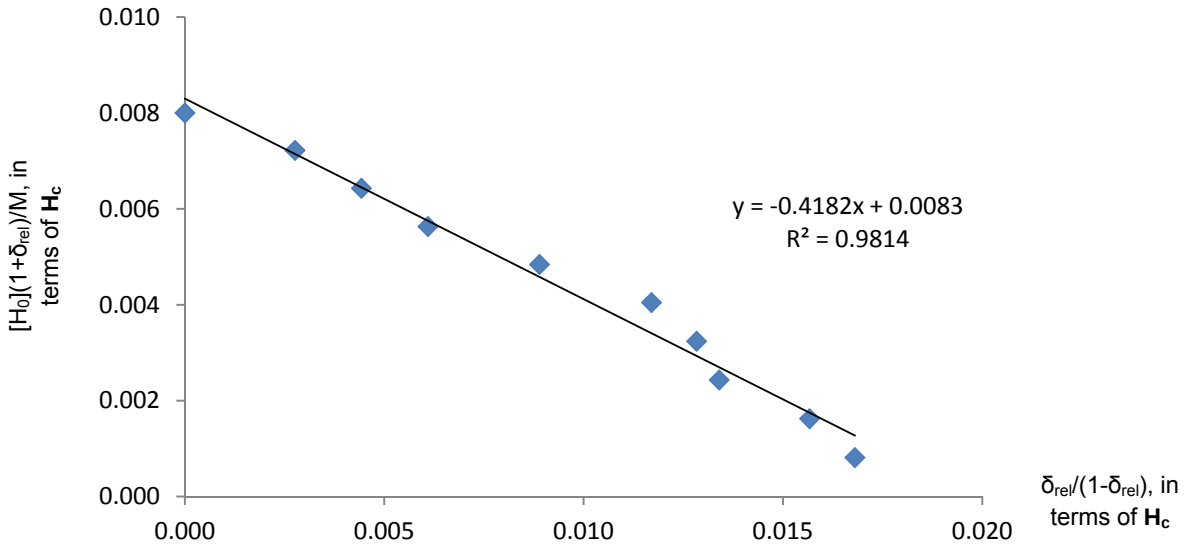

Figure S26. Relationship between $\boldsymbol{\delta_{rel}/(1-\delta_{rel})}$ and $\boldsymbol{[H_0](1+\delta_{rel})}$ for **3** and TBAI interaction in d3-acetonitrile. $[H_0]+[G_0]$ = 8.00 mM. The slope of the fitted line is -1/K, and the intercept is $[H_0]+[G_0]$.

NMR titration of compound 4 and TBACl:

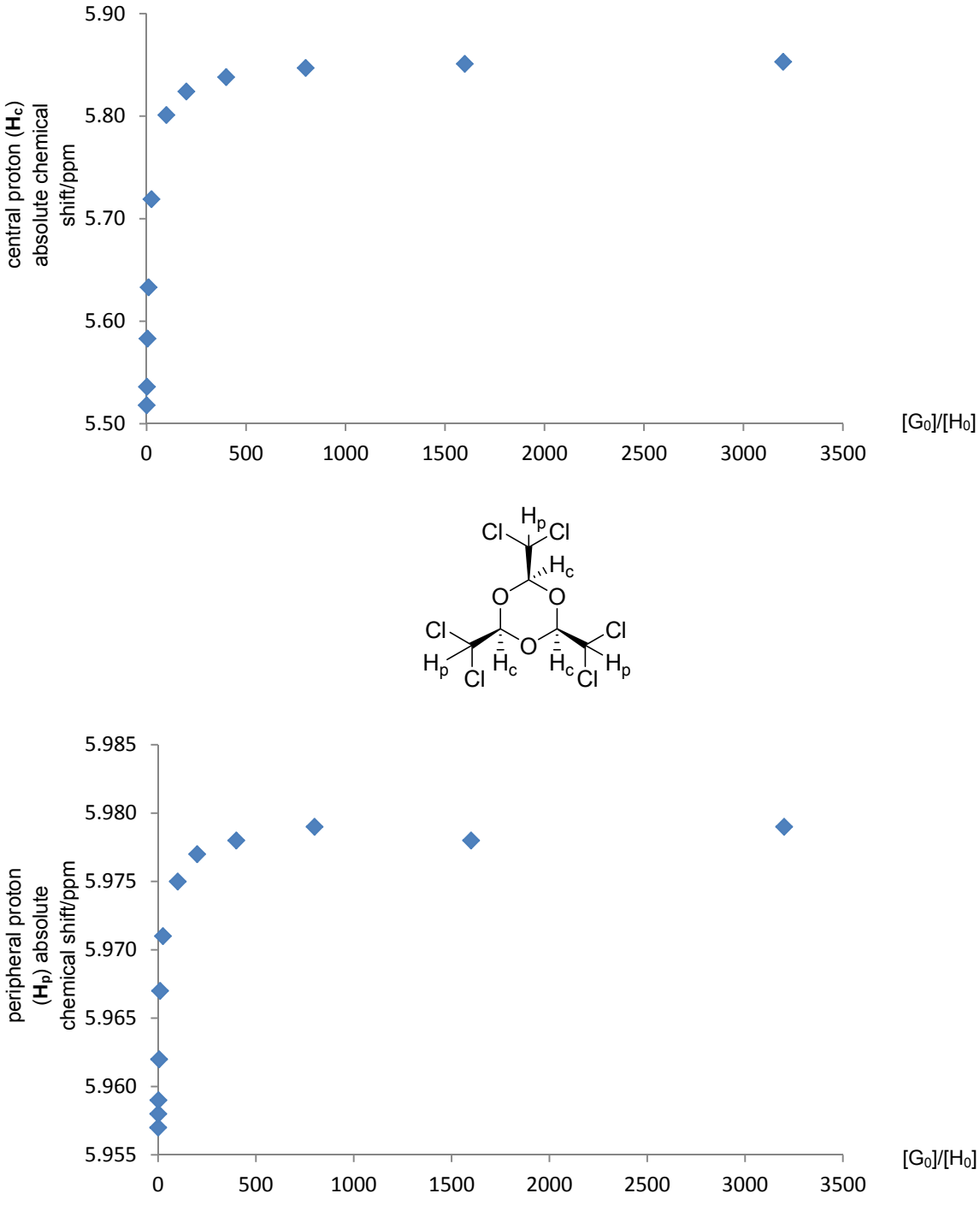

Figure S27. [1]HNMR chemical shifts of **4** and TBACl interaction. 4.00 mM of **4** was titrated by 100.00 mM of TBACl in d3-acetonitrile.

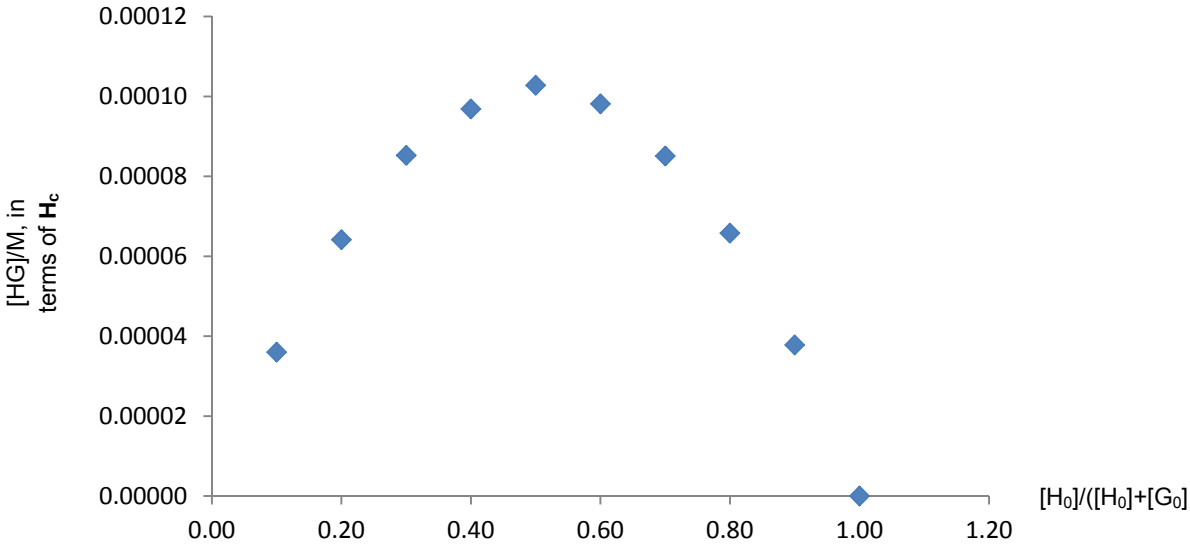

Figure S28. Job Plot of **3** and TBAI interaction in d3-acetonitrile. $[H_0]+[G_0]$ = 8.00 mM.

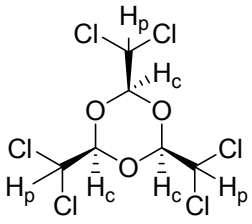

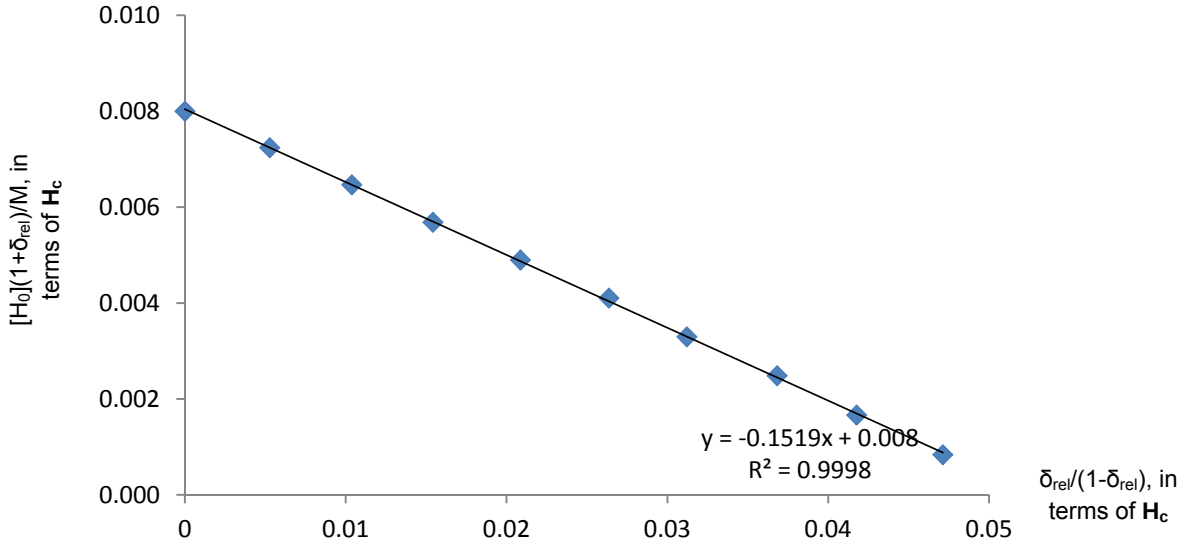

Figure S29. Relationship between $\boldsymbol{\delta_{rel}/(1-\delta_{rel})}$ and $\boldsymbol{[H_0](1+\delta_{rel})}$ for **3** and TBAI interaction in d3-acetonitrile. $[H_0]+[G_0]$ = 8.00 mM. The slope of the fitted line is -1/K, and the intercept is $[H_0]+[G_0]$.

NMR titration of compound 4 and TBABr:

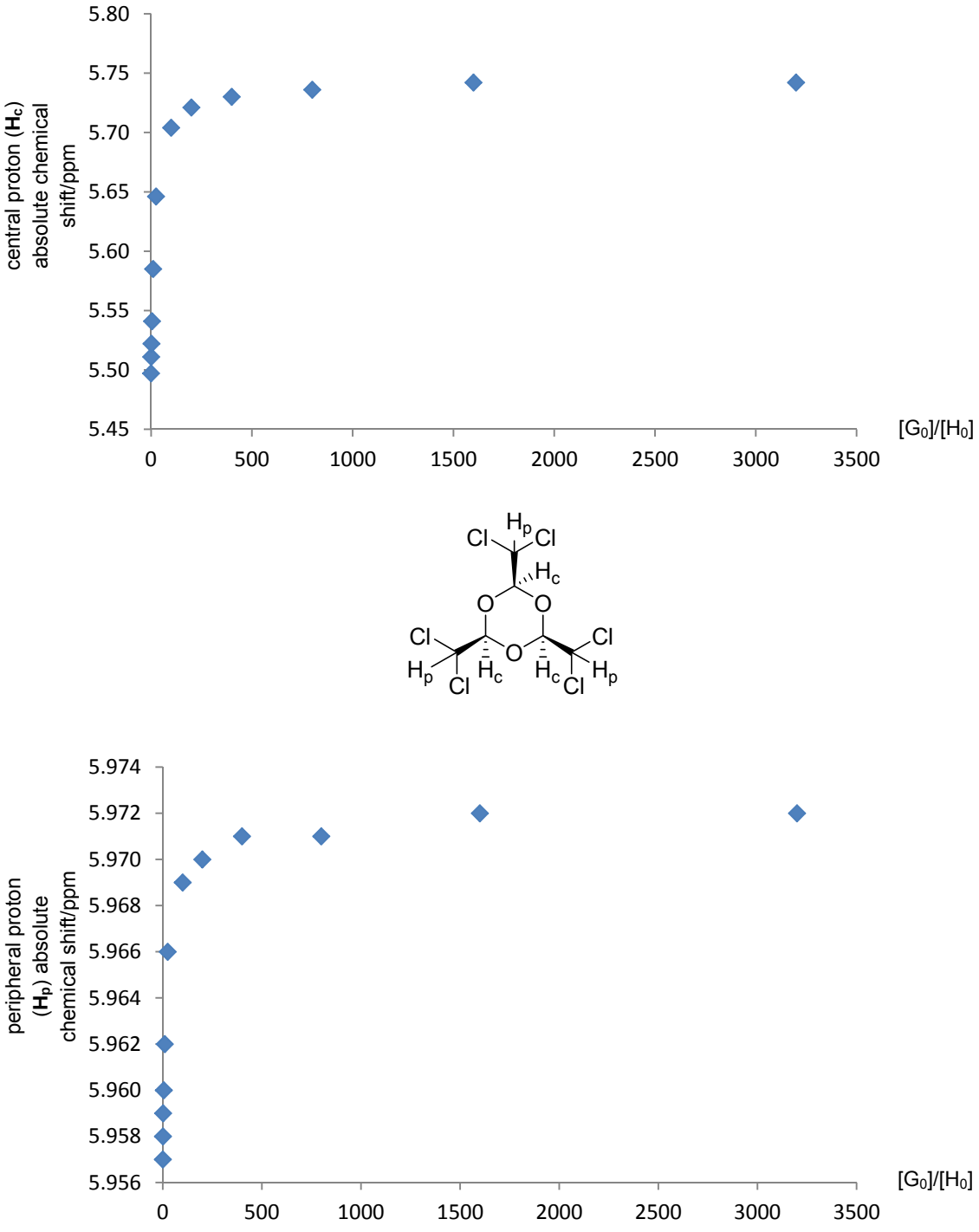

Figure S30. [1]HNMR chemical shifts of **4** and TBABr interaction. 4.00 mM of **4** was titrated by 100.00 mM of TBABr in d3-acetonitrile.

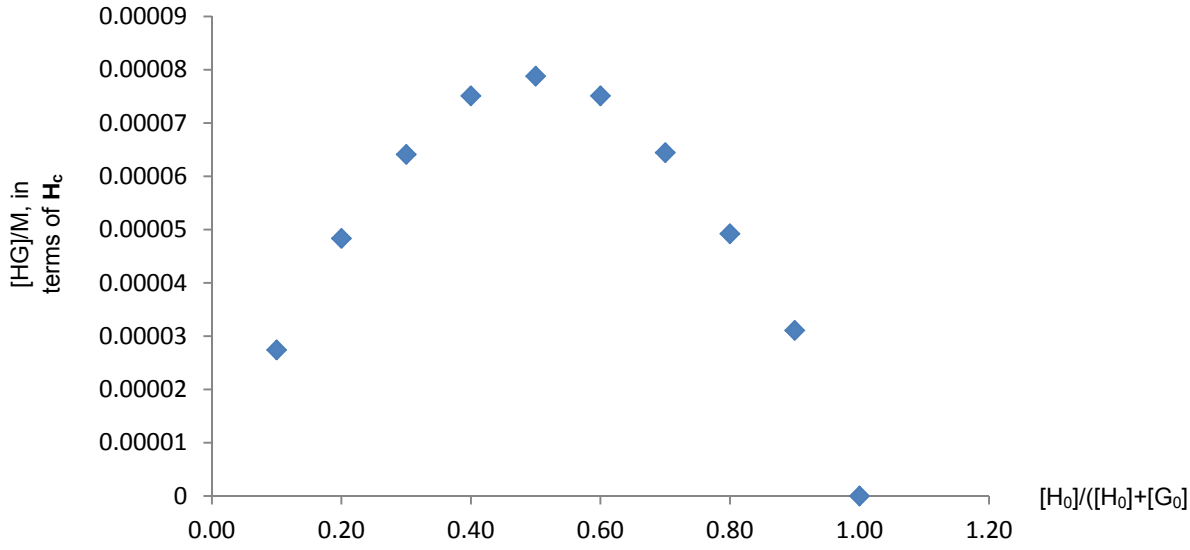

Figure S31. Job Plot of **4** and TBABr interaction in d3-acetonitrile. $[H_0]+[G_0]$ = 8.00 mM.

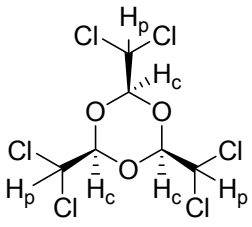

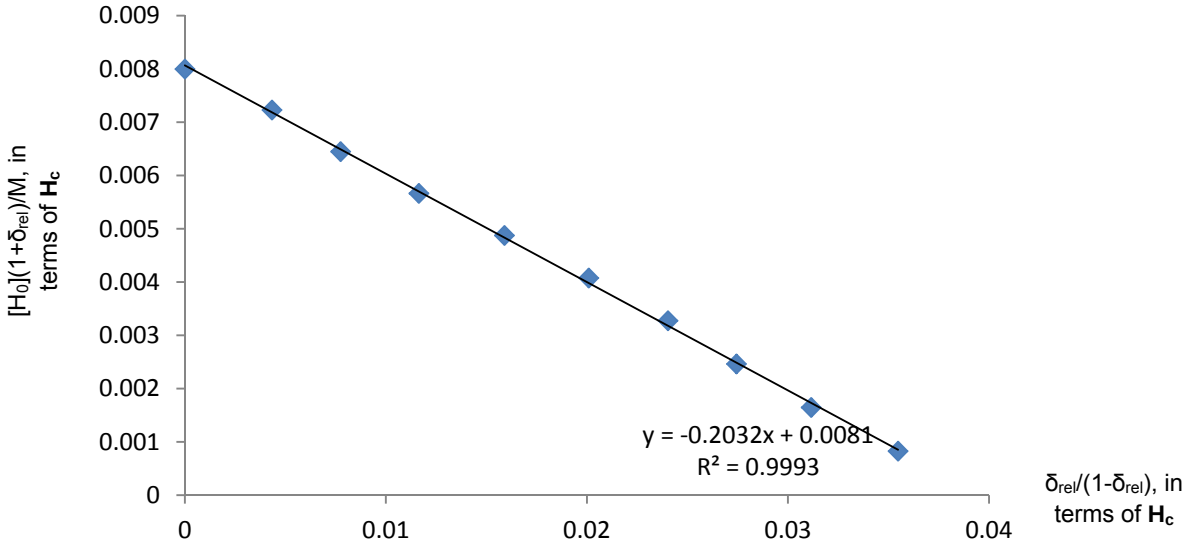

Figure S32. Relationship between $\boldsymbol{\delta_{rel}/(1-\delta_{rel})}$ and $\boldsymbol{[H_0](1+\delta_{rel})}$ for **4** and TBABr interaction in d3-acetonitrile. $[H_0]+[G_0]$ = 8.00 mM. The slope of the fitted line is -1/K, and the intercept is $[H_0]+[G_0]$.

NMR titration of compound 4 and TBAI:

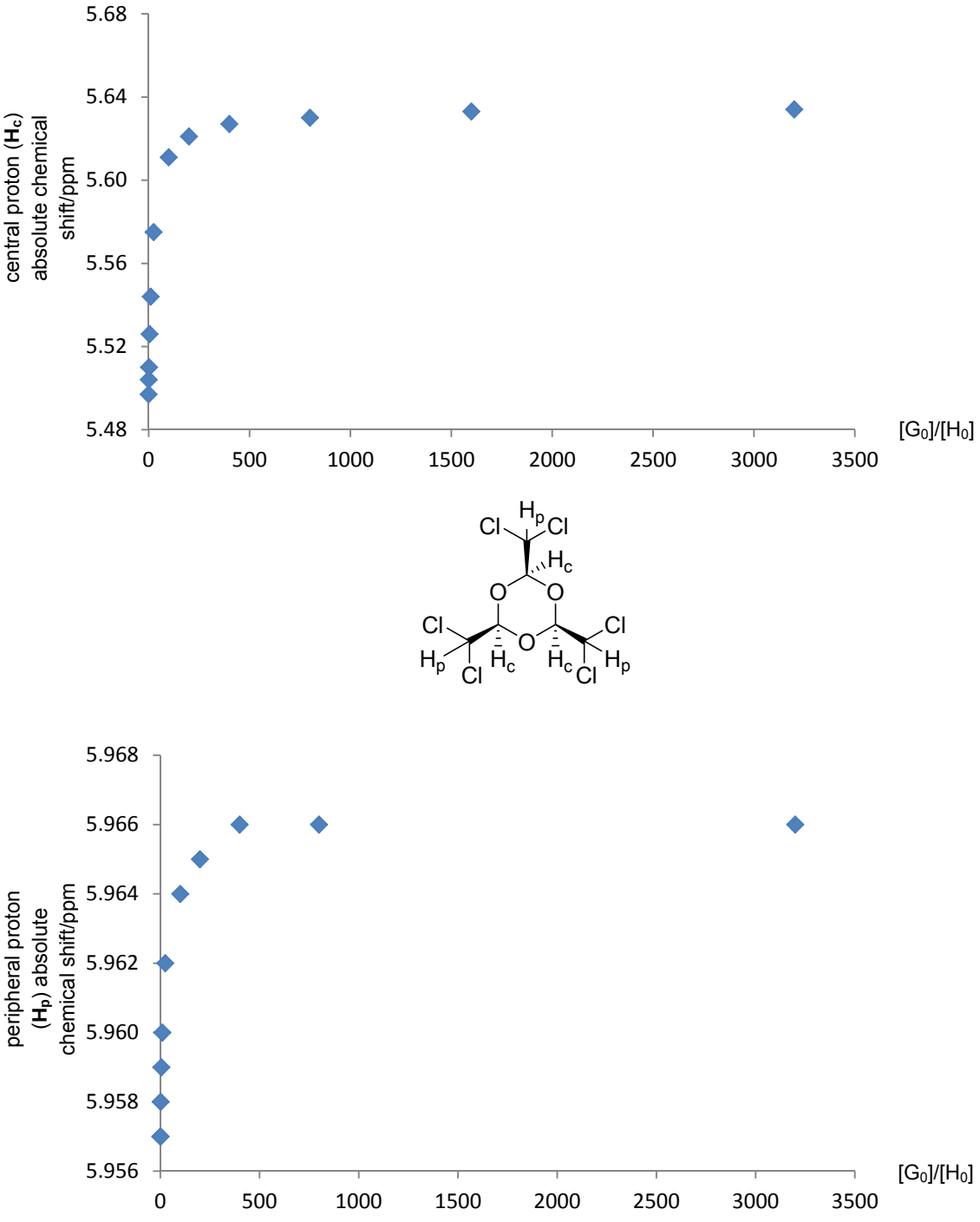

Figure S33. [1]HNMR chemical shifts of **4** and TBAI interaction. 4.00 mM of **4** was titrated by 100.00 mM of TBAI in d3-acetonitrile.

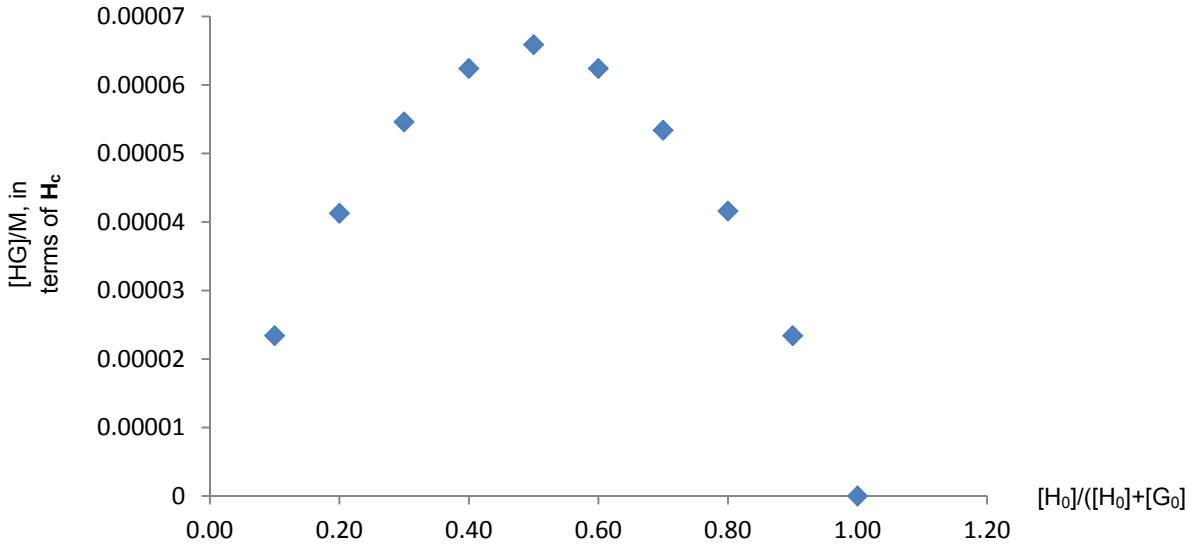

Figure S34. Job Plot of **4** and TBAI interaction in d3-acetonitrile. $[H_0]+[G_0]$ = 8.00 mM.

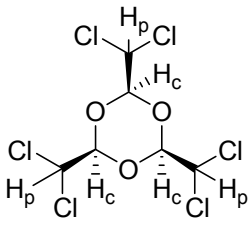

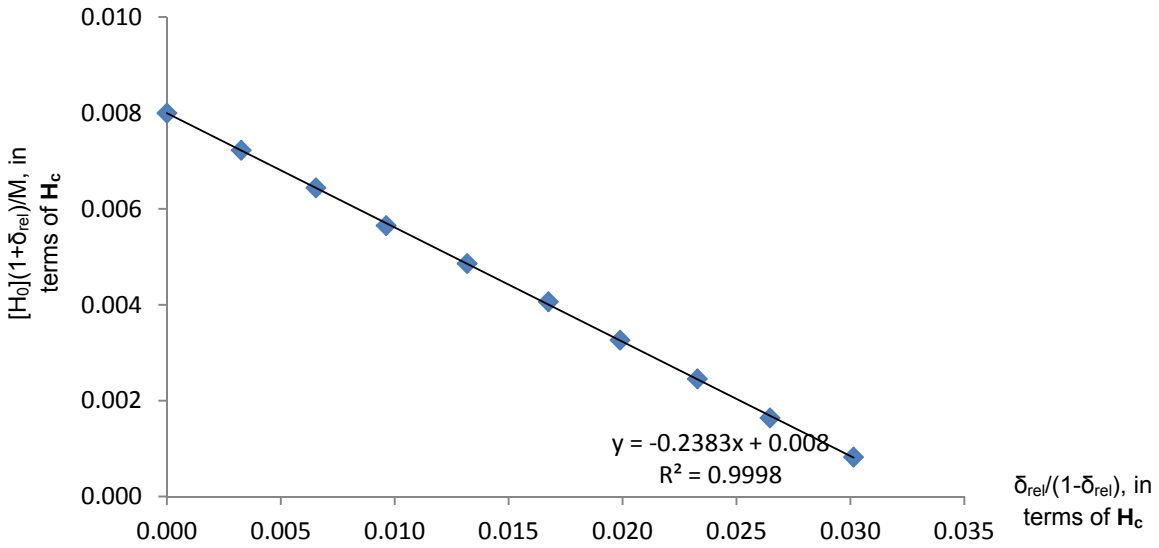

Figure S35. Relationship between $\boldsymbol{\delta_{rel}/(1-\delta_{rel})}$ and $\boldsymbol{[H_0](1+\delta_{rel})}$ for **4** and TBAI interaction in d3-acetonitrile. $[H_0]+[G_0]$ = 8.00 mM. The slope of the fitted line is -1/K, and the intercept is $[H_0]+[G_0]$.

5. Crystallographic Information

(1) Crystallographic data collection and refinement of the structure

A crystal of **3** and **4** were coated with paratone oil and the diffraction data measured at 173 K with Mo Kα radiation on an X-ray diffraction camera system using an imaging plate equipped with a graphite crystal incident beam monochromator. The RapidAuto software[4] was used for data collection and data processing. Structure was solved by direct method and refined by full-matrix least-squares calculation with the SHELXTL software package.[5]

A 2,4,6-tris(chloromethyl)-1,3,5-trioxane (**3**) was observed as an asymmetric unit. All non-hydrogen atoms were refined anisotropically; the hydrogen atoms were assigned isotropic displacement coefficients U(H) = 1.2U (C), and their coordinates were allowed to ride on their respective atoms. Refinement of the structure converged at a final $R1 = 0.0324$ and $wR2 = 0.0808$ for 1946 reflections with $I > 2\sigma(I)$; $R1 = 0.0362$ and $wR2 = 0.0834$ for all 2183 reflections. The largest difference peak and hole were 1.011 and −0.253 e·Å^{-3}, respectively.

A 2,4,6-tris(dichloromethyl)-1,3,5-trioxane (**4**) on a crystallographic three-fold axis with Wyckoff letter *b* symmetry site was observed as an asymmetric unit. All non-hydrogen atoms were refined anisotropically; the hydrogen atoms were assigned isotropic displacement coefficients U(H) = 1.2U (C) and their coordinates were allowed to ride on their respective atoms. Refinement of the structure converged at a final $R1 = 0.0254$ and $wR2 = 0.0592$ for 877 reflections with $I > 2\sigma(I)$; $R1 = 0.0271$ and $wR2 = 0.0604$ for all 926 reflections. The largest difference peak and hole were 0.591 and −0.265 e·Å^{-3}, respectively. The Flack parameter of the structure was refined as 0.21(16).

A summary of the crystal and some crystallography data is given in **Table S1** and **Table S5**. CCDC-961621 and 961620 contains the supplementary crystallographic data for this paper. The data can be obtained free of charge at www.ccdc.cam.ac.uk/conts/retrieving.html or from the Cambridge Crystallographic Data Centre, 12, Union Road, Cambridge CB2 1EZ, UK.

(2) Detailed crystallographic data of 3

Table S3. Crystal data and structure refinement for **3**

Empirical formula	$C_6H_9O_3Cl_3$	
Formula weight	235.48	
Temperature	173(2) K	
Wavelength	0.71073 Å	
Crystal system	Monoclinic	
Space group	$P2_1/n$	
Unit cell dimensions	a = 8.2352(16) Å	α= 90°
	b = 8.6735(17) Å	β= 90.23(3)°
	c = 13.354(3) Å	γ = 90°
Volume	953.8(3) $Å^3$	
Z	4	
Density (calculated)	1.640 Mg/m^3	
Absorption coefficient	0.925 mm^{-1}	
F(000)	480	
Crystal size	0.24 x 0.23 x 0.15 mm^3	
Theta range for data collection	3.05 to 27.45°.	
Index ranges	-10<=h<=10, -11<=k<=11, -16<=l<=17	
Reflections collected	9038	
Independent reflections	2183 [R(int) = 0.0255]	
Completeness to theta = 27.45°	99.6 %	
Absorption correction	Semi-empirical from equivalents	
Max. and min. transmission	0.8737 and 0.8085	
Refinement method	Full-matrix least-squares on F^2	
Data / restraints / parameters	2183 / 0 / 109	
Goodness-of-fit on F2	1.072	
Final R indices [I>2sigma(I)]	R1 = 0.0324, wR2 = 0.0808	
R indices (all data)	R1 = 0.0362, wR2 = 0.0834	
Largest diff. peak and hole	1.011 and –0.253 $e \cdot Å^{-3}$	

Table S4. Atomic coordinates (x 10^4) and equivalent isotropic displacement parameters ($Å^2$x 10^3) for **3**. U(eq) is defined as one third of the trace of the orthogonalized U^{ij} tensor.

	x	y	z	U(eq)
Cl(1)	1283(1)	7942(1)	4911(1)	31(1)
Cl(2)	880(1)	7711(1)	10021(1)	37(1)
Cl(3)	7717(1)	10237(1)	7739(1)	42(1)
O(1)	3420(1)	9320(1)	6577(1)	22(1)
O(2)	1596(1)	8666(1)	7827(1)	23(1)
O(3)	4149(1)	9592(1)	8250(1)	22(1)
C(1)	2169(2)	8291(2)	6855(1)	22(1)
C(2)	744(2)	8502(2)	6153(1)	26(1)
C(3)	2896(2)	8565(2)	8526(1)	21(1)
C(4)	2301(2)	9072(2)	9541(1)	26(1)
C(5)	4714(2)	9213(2)	7277(1)	22(1)
C(6)	5972(2)	10368(2)	6952(1)	27(1)

Table S5. Bond lengths [Å] and angles [°] for **3**

Cl(1)-C(2)	1.7856(18)
Cl(2)-C(4)	1.7834(18)
Cl(3)-C(6)	1.7808(18)
O(1)-C(1)	1.4133(19)
O(1)-C(5)	1.4177(19)
O(2)-C(3)	1.4206(19)
O(2)-C(1)	1.422(2)
O(3)-C(3)	1.413(2)
O(3)-C(5)	1.4207(19)
C(1)-C(2)	1.509(2)
C(3)-C(4)	1.508(2)
C(5)-C(6)	1.507(2)
C(1)-O(1)-C(5)	109.44(12)
C(3)-O(2)-C(1)	109.50(12)
C(3)-O(3)-C(5)	109.58(12)
O(1)-C(1)-O(2)	109.92(13)
O(1)-C(1)-C(2)	109.05(13)
O(2)-C(1)-C(2)	106.20(13)
C(1)-C(2)-Cl(1)	110.37(12)
O(3)-C(3)-O(2)	109.82(12)
O(3)-C(3)-C(4)	106.89(13)
O(2)-C(3)-C(4)	108.97(13)
C(3)-C(4)-Cl(2)	110.24(12)
O(1)-C(5)-O(3)	109.87(12)
O(1)-C(5)-C(6)	106.41(13)
O(3)-C(5)-C(6)	109.78(13)
C(5)-C(6)-Cl(3)	109.95(12)

Table S6. Anisotropic displacement parameters ($Å^2 x\ 10^3$) for **3**. The anisotropic displacement factor exponent takes the form: $-2\pi^2[\ h^2 a^{*2} U^{11} + ... + 2\ h\ k\ a^*\ b^*\ U^{12}\ ]$

	U^{11}	U^{22}	U^{33}	U^{23}	U^{13}	U^{12}
Cl(1)	32(1)	38(1)	24(1)	1(1)	-6(1)	0(1)
Cl(2)	45(1)	39(1)	29(1)	0(1)	8(1)	-15(1)
Cl(3)	25(1)	63(1)	37(1)	-4(1)	-4(1)	-10(1)
O(1)	20(1)	25(1)	22(1)	2(1)	-2(1)	-2(1)
O(2)	19(1)	27(1)	22(1)	2(1)	-1(1)	0(1)
O(3)	21(1)	24(1)	22(1)	-3(1)	1(1)	-2(1)
C(1)	22(1)	21(1)	23(1)	2(1)	-1(1)	-1(1)
C(2)	22(1)	32(1)	24(1)	2(1)	-3(1)	0(1)
C(3)	21(1)	21(1)	22(1)	2(1)	-1(1)	1(1)
C(4)	28(1)	25(1)	24(1)	0(1)	3(1)	-5(1)
C(5)	20(1)	24(1)	21(1)	-2(1)	-1(1)	3(1)
C(6)	21(1)	32(1)	28(1)	-3(1)	0(1)	-3(1)

(3) Detailed crystallographic data of 4

Table S7. Crystal data and structure refinement for **4**

Empirical formula	$C_6H_6O_3Cl_6$	
Formula weight	338.81	
Temperature	173(2) K	
Wavelength	0.71073 Å	
Crystal system	Hexagonal	
Space group	$P6_3$	
Unit cell dimensions	a = 10.0762(14) Å	□α= 90°
	b = 10.0762(14) Å	□β= 90°
	c = 6.9573(14) Å	γ = 120°
Volume	611.74(17) $Å^3$	
Z	2	
Density (calculated)	1.839 Mg/m^3	
Absorption coefficient	1.386 mm^{-1}	
F(000)	336	
Crystal size	0.20 x 0.19 x 0.10 mm^3	
Theta range for data collection	3.75 to 27.45°.	
Index ranges	-13<=h<=13, -13<=k<=11, -9<=l<=8	
Reflections collected	5982	
Independent reflections	926 [R(int) = 0.0222]	
Completeness to theta = 27.45°	99.8 %	
Absorption correction	Semi-empirical from equivalents	
Max. and min. transmission	0.8739 and 0.7691	
Refinement method	Full-matrix least-squares on F^2	
Data / restraints / parameters	926 / 1 / 46	
Goodness-of-fit on F^2	1.229	
Final R indices [I>2sigma(I)]	R1 = 0.0254, wR2 = 0.0592	
R indices (all data)	R1 = 0.0271, wR2 = 0.0604	
Absolute structure parameter	0.21(16)	
Largest diff. peak and hole	0.591 and –0.265 $e \cdot Å^{-3}$	

Table S8. Atomic coordinates (x 10^4) and equivalent isotropic displacement parameters ($Å^2$x 10^3) for **4**. U(eq) is defined as one third of the trace of the orthogonalized U^{ij} tensor.

	x	y	z	U(eq)
Cl(1)	-956(1)	5564(1)	8311(2)	33(1)
Cl(2)	1106(1)	8863(1)	8350(2)	41(1)
C(1)	2115(2)	6862(2)	8130(5)	24(1)
C(2)	866(3)	7061(3)	9050(4)	28(1)
O(12)	1920(2)	5448(2)	8683(4)	36(1)

Table S9. Bond lengths [Å] and angles [°] for **4**.

Cl(1)-C(2)	1.771(3)
Cl(2)-C(2)	1.776(3)
C(1)-O(12)#1	1.391(3)
C(1)-O(12)	1.392(3)
C(1)-C(2)	1.512(3)
O(12)-C(1)#2	1.391(3)
O(12)#1-C(1)-O(12)	112.7(2)
O(12)#1-C(1)-C(2)	108.6(2)
O(12)-C(1)-C(2)	108.5(2)
C(1)-C(2)-Cl(1)	109.97(19)
C(1)-C(2)-Cl(2)	108.81(18)
Cl(1)-C(2)-Cl(2)	110.15(15)
C(1)#2-O(12)-C(1)	112.7(2)

Symmetry transformations used to generate equivalent atoms:

#1 -x+y,-x+1,z #2 -y+1,x-y+1,z

Table S10. Anisotropic displacement parameters ($Å^2 x\ 10^3$)for **4**. The anisotropic displacement factor exponent takes the form: $-2\pi^2[\ h^2 a^{*2} U^{11} + ... + 2\ h\ k\ a^*\ b^*\ U^{12}\ ]$

	U^{11}	U^{22}	U^{33}	U^{23}	U^{13}	U^{12}
Cl(1)	19(1)	35(1)	41(1)	-1(1)	-2(1)	11(1)
Cl(2)	32(1)	29(1)	71(1)	4(1)	3(1)	21(1)
C(1)	20(1)	18(1)	34(2)	-1(1)	1(1)	10(1)
C(2)	24(1)	26(1)	34(1)	-1(1)	2(1)	14(1)
O(12)	20(1)	19(1)	70(2)	5(1)	5(1)	10(1)

[1] S. H. R. *SYBYL 8.1* (**2008**), Tripos Inc., St. Louis, MO 63144 USA.
[2] Case, D.A.; Darden, T.A.; Cheatham, T.E.; III, Simmerling, C.L.; Wang, J.; Duke, R.E.; Luo, R.; Walker, R.C.; Zhang, W.; Merz, K.M.; Roberts, B.; Hayik, S.; Roitberg, A.; Seabra, G.; Swails, J.; Goetz, A.W.; Kolossváry, I.; Wong, K.F.; Paesani, F.; Vanicek, J.; Wolf, R. M.; Liu, J.; Wu, X.; Brozell, S. R.; Steinbrecher, T.; Gohlke, H.; Cai, Q.; Ye, X.; Wang, J.; Hsieh, M.-J.; Cui, G.; Roe, D. R.; Mathews, D. H.; Seetin, M. G.; Salomon-Ferrer, R.; Sagui, C.; Babin, V.; Luchko, T.; Gusarov, S.; Kovalenko, A.; Kollman, P.A. (**2012**), *AMBER 12*, University of California, San Francisco.
[3] Jakalian, A.; Bush, B. L.; Jack, B. D.; Bayly, C.I. *J. Comp. Chem.*, **2000**, *21*, 132-146.
[4] Rapid Auto software, R-Axis series, Cat. No. 9220B101, Rigaku Corporation.
[5] SHELX program: Sheldrick, G. M. *Acta Crystallogr. Sect. A*, **2008**, *64*, 112.